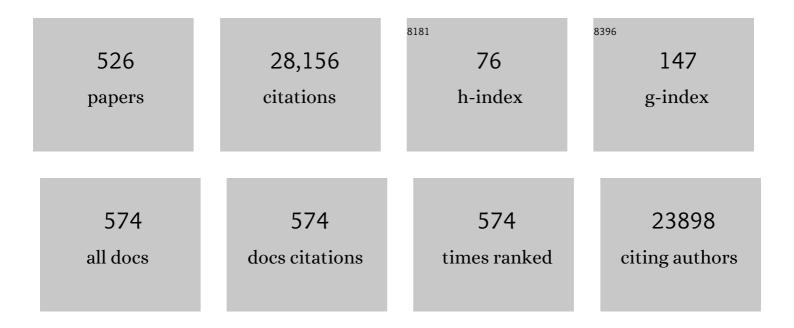
List of Publications by Year in descending order

Source: https://exaly.com/author-pdf/2544654/publications.pdf Version: 2024-02-01



#	Article	IF	CITATIONS
1	FDG PET/CT: EANM procedure guidelines for tumour imaging: version 2.0. European Journal of Nuclear Medicine and Molecular Imaging, 2015, 42, 328-354.	6.4	2,188
2	The Image Biomarker Standardization Initiative: Standardized Quantitative Radiomics for High-Throughput Image-based Phenotyping. Radiology, 2020, 295, 328-338.	7.3	1,869
3	FDG PET and PET/CT: EANM procedure guidelines for tumour PET imaging: version 1.0. European Journal of Nuclear Medicine and Molecular Imaging, 2010, 37, 181-200.	6.4	1,147
4	Imaging biomarker roadmap for cancer studies. Nature Reviews Clinical Oncology, 2017, 14, 169-186.	27.6	792
5	Standards for PET Image Acquisition and Quantitative Data Analysis. Journal of Nuclear Medicine, 2009, 50, 11S-20S.	5.0	720
6	Microglia Activation in Recent-Onset Schizophrenia: A Quantitative (R)-[11C]PK11195 Positron Emission Tomography Study. Biological Psychiatry, 2008, 64, 820-822.	1.3	534
7	89Zr-atezolizumab imaging as a non-invasive approach to assess clinical response to PD-L1 blockade in cancer. Nature Medicine, 2018, 24, 1852-1858.	30.7	468
8	Effects of noise, image resolution, and ROI definition on the accuracy of standard uptake values: a simulation study. Journal of Nuclear Medicine, 2004, 45, 1519-27.	5.0	433
9	Stability of FDG-PET Radiomics features: An integrated analysis of test-retest and inter-observer variability. Acta Oncológica, 2013, 52, 1391-1397.	1.8	353
10	Joint EANM/EANO/RANO practice guidelines/SNMMI procedure standards for imaging of gliomas using PET with radiolabelled amino acids and [18F]FDG: version 1.0. European Journal of Nuclear Medicine and Molecular Imaging, 2019, 46, 540-557.	6.4	348
11	The Netherlands protocol for standardisation and quantification of FDG whole body PET studies in multi-centre trials. European Journal of Nuclear Medicine and Molecular Imaging, 2008, 35, 2320-2333.	6.4	343
12	Δ9-Tetrahydrocannabinol Induces Dopamine Release in the Human Striatum. Neuropsychopharmacology, 2009, 34, 759-766.	5.4	341
13	Whole body PD-1 and PD-L1 positron emission tomography in patients with non-small-cell lung cancer. Nature Communications, 2018, 9, 4664.	12.8	331
14	The effect of SUV discretization in quantitative FDG-PET Radiomics: the need for standardized methodology in tumor texture analysis. Scientific Reports, 2015, 5, 11075.	3.3	318
15	Performance Characteristics of the Digital Biograph Vision PET/CT System. Journal of Nuclear Medicine, 2019, 60, 1031-1036.	5.0	316
16	Performance evaluation of the ECAT HRRT: an LSO-LYSO double layer high resolution, high sensitivity scanner. Physics in Medicine and Biology, 2007, 52, 1505-1526.	3.0	301
17	Quantification of FDG PET studies using standardised uptake values in multi-centre trials: effects of image reconstruction, resolution and ROI definition parameters. European Journal of Nuclear Medicine and Molecular Imaging, 2007, 34, 392-404.	6.4	268
18	89Zr immuno-PET: comprehensive procedures for the production of 89Zr-labeled monoclonal antibodies. Journal of Nuclear Medicine, 2003, 44, 1271-81.	5.0	264

#	Article	IF	CITATIONS
19	Effects of ROI definition and reconstruction method on quantitative outcome and applicability in a response monitoring trial. European Journal of Nuclear Medicine and Molecular Imaging, 2005, 32, 294-301.	6.4	247
20	Repeatability of Radiomic Features in Non-Small-Cell Lung Cancer [18F]FDG-PET/CT Studies: Impact of Reconstruction and Delineation. Molecular Imaging and Biology, 2016, 18, 788-795.	2.6	214
21	Performance of Immuno–Positron Emission Tomography with Zirconium-89-Labeled Chimeric Monoclonal Antibody U36 in the Detection of Lymph Node Metastases in Head and Neck Cancer Patients. Clinical Cancer Research, 2006, 12, 2133-2140.	7.0	207
22	EANM/EARL harmonization strategies in PET quantification: from daily practice to multicentre oncological studies. European Journal of Nuclear Medicine and Molecular Imaging, 2017, 44, 17-31.	6.4	206
23	Early Prediction of Nonprogression in Advanced Non–Small-Cell Lung Cancer Treated With Erlotinib By Using [ <sup>18</sup> F]Fluorodeoxyglucose and [ <sup>18</sup> F]Fluorothymidine Positron Emission Tomography. Journal of Clinical Oncology, 2011, 29, 1701-1708.	1.6	170
24	Standardised FDG uptake: A prognostic factor for inoperable non-small cell lung cancer. European Journal of Cancer, 2005, 41, 1533-1541.	2.8	169
25	Evaluation of a cumulative SUV-volume histogram method for parameterizing heterogeneous intratumoural FDG uptake in non-small cell lung cancer PET studies. European Journal of Nuclear Medicine and Molecular Imaging, 2011, 38, 1636-1647.	6.4	163
26	Relationship of Cerebrospinal Fluid Markers to <sup>11</sup> C-PiB and <sup>18</sup> F-FDDNP Binding. Journal of Nuclear Medicine, 2009, 50, 1464-1470.	5.0	162
27	Quantification, improvement, and harmonization of small lesion detection with state-of-the-art PET. European Journal of Nuclear Medicine and Molecular Imaging, 2017, 44, 4-16.	6.4	156
28	Radiation Dosimetry of <sup>89</sup> Zr-Labeled Chimeric Monoclonal Antibody U36 as Used for Immuno-PET in Head and Neck Cancer Patients. Journal of Nuclear Medicine, 2009, 50, 1828-1836.	5.0	154
29	Repeatability of <sup>18</sup> F-FDG Uptake Measurements in Tumors: A Metaanalysis. Journal of Nuclear Medicine, 2012, 53, 701-708.	5.0	149
30	Quantifying heterogeneity in human tumours using MRI and PET. European Journal of Cancer, 2012, 48, 447-455.	2.8	149
31	Reduced GABAA benzodiazepine receptor binding in veterans with post-traumatic stress disorder. Molecular Psychiatry, 2008, 13, 74-83.	7.9	148
32	Longitudinal Amyloid Imaging Using <sup>11</sup> C-PiB: Methodologic Considerations. Journal of Nuclear Medicine, 2013, 54, 1570-1576.	5.0	148
33	Evaluation of Reference Tissue Models for the Analysis of [11C](R)-PK11195 Studies. Journal of Cerebral Blood Flow and Metabolism, 2006, 26, 1431-1441.	4.3	145
34	Longitudinal imaging of Alzheimer pathology using [11C]PIB, [18F]FDDNP and [18F]FDG PET. European Journal of Nuclear Medicine and Molecular Imaging, 2012, 39, 990-1000.	6.4	145
35	Microglial activation in Alzheimer's disease: an (R)-[11C]PK11195 positron emission tomography study. Neurobiology of Aging, 2013, 34, 128-136.	3.1	145
36	Need for Standardization of <sup>18</sup> F-FDG PET/CT for Treatment Response Assessments. Journal of Nuclear Medicine, 2011, 52, 93S-100S.	5.0	137

#	Article	IF	CITATIONS
37	Characteristics of a new fully programmable blood sampling device for monitoring blood radioactivity during PET. European Journal of Nuclear Medicine and Molecular Imaging, 2001, 28, 81-89.	2.1	136
38	EANM practice guideline/SNMMI procedure standard for dopaminergic imaging in Parkinsonian syndromes 1.0. European Journal of Nuclear Medicine and Molecular Imaging, 2020, 47, 1885-1912.	6.4	134
39	Mutatis Mutandis: Harmonize the Standard!. Journal of Nuclear Medicine, 2012, 53, 1-3.	5.0	133
40	Dopaminergic activity in Tourette syndrome and obsessive-compulsive disorder. European Neuropsychopharmacology, 2013, 23, 1423-1431.	0.7	133
41	Accuracy and precision of pseudo-continuous arterial spin labeling perfusion during baseline and hypercapnia: A head-to-head comparison with 150 H2O positron emission tomography. NeuroImage, 2014, 92, 182-192.	4.2	133
42	Repeatability of <sup>18</sup> F-FDG PET in a Multicenter Phase I Study of Patients with Advanced Gastrointestinal Malignancies. Journal of Nuclear Medicine, 2009, 50, 1646-1654.	5.0	129
43	Partial volume correction strategies for quantitative FDG PET in oncology. European Journal of Nuclear Medicine and Molecular Imaging, 2010, 37, 1679-1687.	6.4	128
44	Partial volume corrected image derived input functions for dynamic PET brain studies: Methodology and validation for [11C]flumazenil. NeuroImage, 2008, 39, 1041-1050.	4.2	127
45	P-Glycoprotein Function at the Blood–Brain Barrier: Effects of Age and Gender. Molecular Imaging and Biology, 2012, 14, 771-776.	2.6	127
46	Microglial activation in healthy aging. Neurobiology of Aging, 2012, 33, 1067-1072.	3.1	125
47	Optimization of Supervised Cluster Analysis for Extracting Reference Tissue Input Curves in ( <i>R</i> )-[ <sup>11</sup> C]PK11195 Brain PET Studies. Journal of Cerebral Blood Flow and Metabolism, 2012, 32, 1600-1608.	4.3	120
48	Detection of Alzheimer Pathology In Vivo Using Both <sup>11</sup> C-PIB and <sup>18</sup> F-FDDNP PET. Journal of Nuclear Medicine, 2009, 50, 191-197.	5.0	119
49	Arterial Spin Labeling Perfusion MRI at Multiple Delay Times: A Correlative Study with H <sub>2</sub> <sup>15</sup> 0 Positron Emission Tomography in Patients with Symptomatic Carotid Artery Occlusion. Journal of Cerebral Blood Flow and Metabolism, 2010, 30, 222-229.	4.3	117
50	Experimental and clinical evaluation of iterative reconstruction (OSEM) in dynamic PET: quantitative characteristics and effects on kinetic modeling. Journal of Nuclear Medicine, 2001, 42, 808-17.	5.0	114
51	Long-Lived Positron Emitters Zirconium-89 and Iodine-124 for Scouting of Therapeutic Radioimmunoconjugates with PET. Cancer Biotherapy and Radiopharmaceuticals, 2003, 18, 655-661.	1.0	111
52	Amyloid burden and metabolic function in early-onset Alzheimer's disease: parietal lobe involvement. Brain, 2012, 135, 2115-2125.	7.6	109
53	(R)- and (S)-[11C]verapamil as PET-tracers for measuring P-glycoprotein function: in vitro and in vivo evaluation. Nuclear Medicine and Biology, 2003, 30, 747-751.	0.6	106
54	89Zr-cetuximab PET imaging in patients with advanced colorectal cancer. Oncotarget, 2015, 6, 30384-30393.	1.8	106

4

#	Article	IF	CITATIONS
55	<sup>18</sup> F-FDG PET as a Tool to Predict the Clinical Outcome of Infliximab Treatment of Rheumatoid Arthritis: An Explorative Study. Journal of Nuclear Medicine, 2011, 52, 77-80.	5.0	104
56	EANM/EARL FDG-PET/CT accreditation - summary results from the first 200 accredited imaging systems. European Journal of Nuclear Medicine and Molecular Imaging, 2018, 45, 412-422.	6.4	104
57	Evaluation of Basis Function and Linear Least Squares Methods for Generating Parametric Blood Flow Images Using 15O-Water and Positron Emission Tomography. Molecular Imaging and Biology, 2005, 7, 273-285.	2.6	101
58	Determinants of coronary microvascular dysfunction in symptomatic hypertrophic cardiomyopathy. American Journal of Physiology - Heart and Circulatory Physiology, 2008, 294, H986-H993.	3.2	101
59	Feasibility of state of the art PET/CT systems performance harmonisation. European Journal of Nuclear Medicine and Molecular Imaging, 2018, 45, 1344-1361.	6.4	100
60	Differential effect of <i>APOE</i> genotype on amyloid load and glucose metabolism in AD dementia. Neurology, 2013, 80, 359-365.	1.1	99
61	Quantification of [ <sup>18</sup> F]DPA-714 Binding in the Human Brain: Initial Studies in Healthy Controls and Alzheimer'S Disease Patients. Journal of Cerebral Blood Flow and Metabolism, 2015, 35, 766-772.	4.3	99
62	Amygdala activity in obsessive-compulsive disorder with contamination fear: a study with oxygen-15 water positron emission tomography. Psychiatry Research - Neuroimaging, 2004, 132, 225-237.	1.8	98
63	Repeatability of Metabolically Active Volume Measurements with <sup>18</sup> F-FDG and <sup>18</sup> F-FLT PET in Non–Small Cell Lung Cancer. Journal of Nuclear Medicine, 2010, 51, 1870-1877.	5.0	98
64	Noninvasive imaging of macrophages in rheumatoid synovitis using <sup>11</sup> Câ€( <i>R</i> )â€₱K11195 and positron emission tomography. Arthritis and Rheumatism, 2008, 58, 3350-3355.	6.7	97
65	Impact of [18F]FDG PET imaging parameters on automatic tumour delineation: need for improved tumour delineation methodology. European Journal of Nuclear Medicine and Molecular Imaging, 2011, 38, 2136-2144.	6.4	96
66	A Guide to ComBat Harmonization of Imaging Biomarkers in Multicenter Studies. Journal of Nuclear Medicine, 2022, 63, 172-179.	5.0	96
67	Fluorodeoxyglucose Positron Emission Tomography for Evaluating Early Response During Neoadjuvant Chemoradiotherapy in Patients With Potentially Curable Esophageal Cancer. Annals of Surgery, 2011, 253, 56-63.	4.2	94
68	Summary of the UPICT Protocol for <sup>18</sup> F-FDG PET/CT Imaging in Oncology Clinical Trials. Journal of Nuclear Medicine, 2015, 56, 955-961.	5.0	93
69	Image-derived input functions for determination of MRGlu in cardiac (18)F-FDG PET scans. Journal of Nuclear Medicine, 2001, 42, 1622-9.	5.0	88
70	Evaluation of Tracer Kinetic Models for Quantification of P-Glycoprotein Function using (R)-[11C]Verapamil and PET. Journal of Cerebral Blood Flow and Metabolism, 2007, 27, 424-433.	4.3	87
71	Simplified parametric methods for [11C]PIB studies. NeuroImage, 2008, 42, 76-86.	4.2	85
72	Machine learning-based analysis of [18F]DCFPyL PET radiomics for risk stratification in primary prostate cancer. European Journal of Nuclear Medicine and Molecular Imaging, 2021, 48, 340-349.	6.4	84

#	Article	IF	CITATIONS
73	New Method to Obtain the Midplane Dose Using Portal In Vivo Dosimetry. International Journal of Radiation Oncology Biology Physics, 1998, 41, 465-474.	0.8	83
74	Evaluation of strategies towards harmonization of FDG PET/CT studies in multicentre trials: comparison of scanner validation phantoms and data analysis procedures. European Journal of Nuclear Medicine and Molecular Imaging, 2013, 40, 1507-1515.	6.4	82
75	Repeatability of Metabolically Active Tumor Volume Measurements with FDG PET/CT in Advanced Gastrointestinal Malignancies: A Multicenter Study. Radiology, 2014, 273, 539-548.	7.3	82
76	EANM procedure guidelines for brain PET imaging using [18F]FDG, version 3. European Journal of Nuclear Medicine and Molecular Imaging, 2022, 49, 632-651.	6.4	82
77	Optimization algorithms and weighting factors for analysis of dynamic PET studies. Physics in Medicine and Biology, 2006, 51, 4217-4232.	3.0	81
78	Repeatability of <sup>18</sup> Fâ€ <scp>FDG PET</scp> radiomic features: A phantom study to explore sensitivity to image reconstruction settings, noise, and delineation method. Medical Physics, 2019, 46, 665-678.	3.0	81
79	Quantitative Imaging Test Approval and Biomarker Qualification: Interrelated but Distinct Activities. Radiology, 2011, 259, 875-884.	7.3	80
80	Cerebral perfusion and glucose metabolism in Alzheimer's disease and frontotemporal dementia: two sides of the same coin?. European Radiology, 2015, 25, 3050-3059.	4.5	80
81	Reduced parahippocampal and lateral temporal GABAA-[11C]flumazenil binding in major depression: preliminary results. European Journal of Nuclear Medicine and Molecular Imaging, 2010, 37, 565-574.	6.4	79
82	Accurate PET/MR Quantification Using Time of Flight MLAA Image Reconstruction. Molecular Imaging and Biology, 2014, 16, 469-477.	2.6	78
83	Transmission dosimetry with a liquid-filled electronic portal imaging device. International Journal of Radiation Oncology Biology Physics, 1996, 34, 931-941.	0.8	76
84	Comparative Study With New Accuracy Metrics for Target Volume Contouring in PET Image Guided Radiation Therapy. IEEE Transactions on Medical Imaging, 2012, 31, 2006-2024.	8.9	75
85	Optimized dose regimen for whole-body FDG-PET imaging. EJNMMI Research, 2013, 3, 63.	2.5	73
86	Widespread and Prolonged Increase in ( <i>R</i> )- <sup>11</sup> C-PK11195 Binding After Traumatic Brain Injury. Journal of Nuclear Medicine, 2011, 52, 1235-1239.	5.0	72
87	Quantitative 89Zr immuno-PET for in vivo scouting of 90Y-labeled monoclonal antibodies in xenograft-bearing nude mice. Journal of Nuclear Medicine, 2003, 44, 1663-70.	5.0	72
88	Reproducibility of quantitative 18F-3′-deoxy-3′-fluorothymidine measurements using positron emission tomography. European Journal of Nuclear Medicine and Molecular Imaging, 2009, 36, 389-395.	6.4	71
89	In vivo imaging of the 18-kDa translocator protein (TSPO) with [18F]FEDAA1106 and PET does not show increased binding in Alzheimer's disease patients. European Journal of Nuclear Medicine and Molecular Imaging, 2013, 40, 921-931.	6.4	71
90	Development of a Tracer Kinetic Plasma Input Model for (R)-[11C]PK11195 Brain Studies. Journal of Cerebral Blood Flow and Metabolism, 2005, 25, 842-851.	4.3	68

#	Article	IF	CITATIONS
91	Dynamic risk assessment based on positron emission tomography scanning in diffuse large B-cell lymphoma: Post-hoc analysis from the PETAL trial. European Journal of Cancer, 2020, 124, 25-36.	2.8	67
92	Impact of anatomical and functional severity of coronary atherosclerotic plaques on the transmural perfusion gradient: a [150]H2O PET study. European Heart Journal, 2014, 35, 2094-2105.	2.2	66
93	Quantitative Analysis of Response to Treatment with Erlotinib in Advanced Non–Small Cell Lung Cancer Using 18F-FDG and 3′-Deoxy-3′-18F-Fluorothymidine PET. Journal of Nuclear Medicine, 2011, 52, 1871-1877.	5.0	65
94	Measuring response to therapy using FDG PET: semi-quantitative and full kinetic analysis. European Journal of Nuclear Medicine and Molecular Imaging, 2011, 38, 832-842.	6.4	63
95	Multicenter Harmonization of <sup>89</sup> Zr PET/CT Performance. Journal of Nuclear Medicine, 2014, 55, 264-267.	5.0	63
96	In vivo (R)-[11C]PK11195 PET imaging of 18kDa translocator protein in recent onset psychosis. NPJ Schizophrenia, 2016, 2, 16031.	3.6	63
97	First clinical tests using a liquid-filled electronic portal imaging device and a convolution model for the werification of the midplane dose. Radiotherapy and Oncology, 1998, 47, 303-312.	0.6	62
98	Test-retest variability of quantitative [11C]PIB studies in Alzheimer's disease. European Journal of Nuclear Medicine and Molecular Imaging, 2009, 36, 1629-1638.	6.4	62
99	Investigating the state-of-the-art in whole-body MR-based attenuation correction: an intra-individual, inter-system, inventory study on three clinical PET/MR systems. Magnetic Resonance Materials in Physics, Biology, and Medicine, 2016, 29, 75-87.	2.0	62
100	18F-FDG PET baseline radiomics features improve the prediction of treatment outcome in diffuse large B-cell lymphoma. European Journal of Nuclear Medicine and Molecular Imaging, 2022, 49, 932-942.	6.4	62
101	A convolution model to convert transmission dose images to exit dose distributions. Medical Physics, 1997, 24, 189-199.	3.0	61
102	Validated imaging biomarkers as decision-making tools in clinical trials and routine practice: current status and recommendations from the EIBALL* subcommittee of the European Society of Radiology (ESR). Insights Into Imaging, 2019, 10, 87.	3.4	61
103	Effects of Image Characteristics on Performance of Tumor Delineation Methods: A Test–Retest Assessment. Journal of Nuclear Medicine, 2011, 52, 1550-1558.	5.0	60
104	RaCaT: An open source and easy to use radiomics calculator tool. PLoS ONE, 2019, 14, e0212223.	2.5	60
105	Pelvic lymph-node staging with 18F-DCFPyL PET/CT prior to extended pelvic lymph-node dissection in primary prostate cancer - the SALT trial European Journal of Nuclear Medicine and Molecular Imaging, 2021, 48, 509-520.	6.4	60
106	HRRT Versus HR+ Human Brain PET Studies: An Interscanner Test–Retest Study. Journal of Nuclear Medicine, 2009, 50, 693-702.	5.0	59
107	Increased cerebral (R)-[11C]PK11195 uptake and glutamate release in a rat model of traumatic brain injury: a longitudinal pilot study. Journal of Neuroinflammation, 2011, 8, 67.	7.2	59
108	Improved detection of diffuse glioma infiltration with imaging combinations: a diagnostic accuracy study. Neuro-Oncology, 2020, 22, 412-422.	1.2	59

#	Article	IF	CITATIONS
109	Assessment of tumour size in PET/CT lung cancer studies: PET- and CT-based methods compared to pathology. EJNMMI Research, 2012, 2, 56.	2.5	57
110	Current Image Acquisition Options in PET/MR. Seminars in Nuclear Medicine, 2015, 45, 192-200.	4.6	57
111	Image Quality and Semiquantitative Measurements on the Biograph Vision PET/CT System: Initial Experiences and Comparison with the Biograph mCT. Journal of Nuclear Medicine, 2020, 61, 129-135.	5.0	56
112	18FDG uptake in oesophageal adenocarcinoma: linking biology and outcome. Journal of Cancer Research and Clinical Oncology, 2008, 134, 227-236.	2.5	55
113	Day-to-Day Test–Retest Variability of CBF, CMRO2, and OEF Measurements Using Dynamic 15O PET Studies. Molecular Imaging and Biology, 2011, 13, 759-768.	2.6	55
114	18F-FDG PET image biomarkers improve prediction of late radiation-induced xerostomia. Radiotherapy and Oncology, 2018, 126, 89-95.	0.6	55
115	Multitracer model for staging cortical amyloid deposition using PET imaging. Neurology, 2020, 95, e1538-e1553.	1.1	55
116	Experimental Multicenter and Multivendor Evaluation of the Performance of PET Radiomic Features Using 3-Dimensionally Printed Phantom Inserts. Journal of Nuclear Medicine, 2020, 61, 469-476.	5.0	54
117	Quantification of PD-L1 Expression with <sup>18</sup> F-BMS-986192 PET/CT in Patients with Advanced-Stage Non–Small Cell Lung Cancer. Journal of Nuclear Medicine, 2020, 61, 1455-1460.	5.0	54
118	Two-dimensional exit dosimetry using a liquid-filled electronic portal imaging device and a convolution model. Radiotherapy and Oncology, 1997, 44, 149-157.	0.6	53
119	Evaluation of Reference Regions for <i>(R)</i> -[ <sup>11</sup> C]PK11195 Studies in Alzheimer's Disease and Mild Cognitive Impairment. Journal of Cerebral Blood Flow and Metabolism, 2007, 27, 1965-1974.	4.3	53
120	Repeatability of Quantitative Whole-Body <sup>18</sup> F-FDG PET/CT Uptake Measures as Function of Uptake Interval and Lesion Selection in Non–Small Cell Lung Cancer Patients. Journal of Nuclear Medicine, 2016, 57, 1343-1349.	5.0	53
121	Automated Segmentation of Baseline Metabolic Total Tumor Burden in Diffuse Large B-Cell Lymphoma: Which Method Is Most Successful? A Study on Behalf of the PETRA Consortium. Journal of Nuclear Medicine, 2021, 62, 332-337.	5.0	53
122	Incorporating radiomics into clinical trials: expert consensus endorsed by the European Society of Radiology on considerations for data-driven compared to biologically driven quantitative biomarkers. European Radiology, 2021, 31, 6001-6012.	4.5	53
123	Proposed New Dynamic Prognostic Index for Diffuse Large B-Cell Lymphoma: International Metabolic Prognostic Index. Journal of Clinical Oncology, 2022, 40, 2352-2360.	1.6	53
124	High-quality 124I-labelled monoclonal antibodies for use as PET scouting agents prior to 131I-radioimmunotherapy. European Journal of Nuclear Medicine and Molecular Imaging, 2004, 31, 1645-1652.	6.4	52
125	Comparison of Plasma Input and Reference Tissue Models for Analysing [ <sup>11</sup> C]flumazenil Studies. Journal of Cerebral Blood Flow and Metabolism, 2008, 28, 579-587.	4.3	52
126	Integration of FDG- PET/CT into external beam radiation therapy planning. Nuklearmedizin - NuclearMedicine, 2012, 51, 140-153.	0.7	52

#	Article	IF	CITATIONS
127	Does Myocardial Fibrosis Hinder Contractile Function and Perfusion in Idiopathic Dilated Cardiomyopathy? PET and MR Imaging Study. Radiology, 2006, 240, 380-388.	7.3	51
128	Image-derived input functions for PET brain studies. European Journal of Nuclear Medicine and Molecular Imaging, 2009, 36, 463-471.	6.4	51
129	Long-term effects of amyloid, hypometabolism, and atrophy on neuropsychological functions. Neurology, 2014, 82, 1768-1775.	1.1	51
130	Quality control for quantitative multicenter wholeâ€body PET/MR studies: A NEMA image quality phantom study with three current PET/MR systems. Medical Physics, 2015, 42, 5961-5969.	3.0	51
131	The dose response relationship of a liquid-filled electronic portal imaging device. Medical Physics, 1996, 23, 1601-1611.	3.0	50
132	Radiomics analysis of pre-treatment [18F]FDG PET/CT for patients with metastatic colorectal cancer undergoing palliative systemic treatment. European Journal of Nuclear Medicine and Molecular Imaging, 2018, 45, 2307-2317.	6.4	50
133	Bone formation rather than inflammation reflects Ankylosing Spondylitis activity on PET-CT: a pilot study. Arthritis Research and Therapy, 2012, 14, R71.	3.5	49
134	Impact of PET/CT image reconstruction methods and liver uptake normalization strategies on quantitative image analysis. European Journal of Nuclear Medicine and Molecular Imaging, 2016, 43, 249-258.	6.4	49
135	The QIBA Profile for FDG PET/CT as an Imaging Biomarker Measuring Response to Cancer Therapy. Radiology, 2020, 294, 647-657.	7.3	49
136	Outcome prediction of head and neck squamous cell carcinoma by MRI radiomic signatures. European Radiology, 2020, 30, 6311-6321.	4.5	49
137	PET imaging of zirconium-89 labelled cetuximab: A phase I trial in patients with head and neck and lung cancer. Radiotherapy and Oncology, 2017, 122, 267-273.	0.6	48
138	Androgen and Estrogen Receptor Imaging in Metastatic Breast Cancer Patients as a Surrogate for Tissue Biopsies. Journal of Nuclear Medicine, 2017, 58, 1906-1912.	5.0	48
139	Monitoring of response to pre-operative chemoradiation in combination with hyperthermia in oesophageal cancer by FDG-PET. International Journal of Hyperthermia, 2006, 22, 149-160.	2.5	47
140	Tumor Lesion Glycolysis and Tumor Lesion Proliferation for Response Prediction and Prognostic Differentiation in Patients With Advanced Non–Small Cell Lung Cancer Treated With Erlotinib. Clinical Nuclear Medicine, 2012, 37, 1058-1064.	1.3	47
141	Guidelines for the content and format of PET brain data in publications and archives: A consensus paper. Journal of Cerebral Blood Flow and Metabolism, 2020, 40, 1576-1585.	4.3	47
142	In vivo tau pathology is associated with synaptic loss and altered synaptic function. Alzheimer's Research and Therapy, 2021, 13, 35.	6.2	47
143	Comparative biodistribution analysis across four different <sup>89</sup> Zr-monoclonal antibody tracers—The first step towards an imaging warehouse. Theranostics, 2018, 8, 4295-4304.	10.0	46
144	Importance of fluorodeoxyglucose-positron emission tomography (FDG-PET) and endoscopic ultrasonography parameters in predicting survival following surgery for esophageal cancer. Endoscopy, 2008, 40, 464-471.	1.8	45

#	Article	IF	CITATIONS
145	Differential association of [ <sup>11</sup> C]PIB and [ <sup>18</sup> F]FDDNP binding with cognitive impairment. Neurology, 2009, 73, 2079-2085.	1.1	45
146	Reproducibility of quantitative (R)-[11C]verapamil studies. EJNMMI Research, 2012, 2, 1.	2.5	45
147	Reproducibility of Tumor Perfusion Measurements Using <sup>15</sup> O-Labeled Water and PET. Journal of Nuclear Medicine, 2008, 49, 1763-1768.	5.0	44
148	Study of <sup>89</sup> Zr-Pembrolizumab PET/CT in Patients With Advanced-Stage Non–Small Cell Lung Cancer. Journal of Nuclear Medicine, 2022, 63, 362-367.	5.0	44
149	Predictive value of early and late residual 18F-fluorodeoxyglucose and 18F-fluorothymidine uptake using different SUV measurements in patients with non-small-cell lung cancer treated with erlotinib. European Journal of Nuclear Medicine and Molecular Imaging, 2012, 39, 1117-1127.	6.4	43
150	Pilot study of 89Zr-bevacizumab positron emission tomography in patients with advanced non-small cell lung cancer. EJNMMI Research, 2014, 4, 35.	2.5	43
151	Functional imaging early during (chemo)radiotherapy for response prediction in head and neck squamous cell carcinoma; a systematic review. Oral Oncology, 2019, 88, 75-83.	1.5	43
152	Quantification of Tau Load Using [18F]AV1451 PET. Molecular Imaging and Biology, 2017, 19, 963-971.	2.6	42
153	Diagnostic Accuracy of Neuroimaging to Delineate Diffuse Gliomas within the Brain: A Meta-Analysis. American Journal of Neuroradiology, 2017, 38, 1884-1891.	2.4	42
154	The engagement of FDG PET/CT image quality and harmonized quantification: from competitive to complementary. European Journal of Nuclear Medicine and Molecular Imaging, 2016, 43, 1-4.	6.4	41
155	Image Quality and Activity Optimization in Oncologic <sup>18</sup> F-FDG PET Using the Digital Biograph Vision PET/CT System. Journal of Nuclear Medicine, 2020, 61, 764-771.	5.0	41
156	Perfusable tissue index as a potential marker of fibrosis in patients with idiopathic dilated cardiomyopathy. Journal of Nuclear Medicine, 2004, 45, 1299-304.	5.0	41
157	Accuracy of 3-Dimensional Reconstruction Algorithms for the High-Resolution Research Tomograph. Journal of Nuclear Medicine, 2009, 50, 72-80.	5.0	40
158	Neurophysiological Effects of Sleep Deprivation in Healthy Adults, a Pilot Study. PLoS ONE, 2015, 10, e0116906.	2.5	40
159	PET/CT-Derived Whole-Body and Bone Marrow Dosimetry of <sup>89</sup> Zr-Cetuximab. Journal of Nuclear Medicine, 2015, 56, 249-254.	5.0	40
160	Associations between quantitative [18F]flortaucipir tau PET and atrophy across the Alzheimer's disease spectrum. Alzheimer's Research and Therapy, 2019, 11, 60.	6.2	40
161	Discordant amyloid-β PET and CSF biomarkers and its clinical consequences. Alzheimer's Research and Therapy, 2019, 11, 78.	6.2	40
162	Optimal timing and criteria of interim PET in DLBCL: a comparative study of 1692 patients. Blood Advances, 2021, 5, 2375-2384.	5.2	40

#	Article	IF	CITATIONS
163	Image-Derived Input Function for Human Brain Using High Resolution PET Imaging with [11C](R)-rolipram and [11C]PBR28. PLoS ONE, 2011, 6, e17056.	2.5	40
164	Characterization of a single LSO crystal layer High Resolution Research Tomograph. Physics in Medicine and Biology, 2003, 48, 429-448.	3.0	39
165	Cerebral microglia activation in hepatitis C virus infection correlates to cognitive dysfunction. Journal of Viral Hepatitis, 2016, 23, 348-357.	2.0	39
166	Technical and instrumentational foundations of PET/MRI. European Journal of Radiology, 2017, 94, A3-A13.	2.6	39
167	The Role of <sup>89</sup> Zr-Immuno-PET in Navigating and Derisking the Development of Biopharmaceuticals. Journal of Nuclear Medicine, 2021, 62, 438-445.	5.0	39
168	Combined PET/MR: Where Are We Now? Summary Report of the Second International Workshop on PET/MR Imaging April 8–12, 2013, Tubingen, Germany. Molecular Imaging and Biology, 2014, 16, 295-310.	2.6	38
169	<sup>89</sup> Zr-Immuno-PET: Toward a Noninvasive Clinical Tool to Measure Target Engagement of Therapeutic Antibodies In Vivo. Journal of Nuclear Medicine, 2019, 60, 1825-1832.	5.0	38
170	Predictive value of quantitative diffusion-weighted imaging and 18-F-FDG-PET in head and neck squamous cell carcinoma treated by (chemo)radiotherapy. European Journal of Radiology, 2019, 113, 39-50.	2.6	38
171	89Zr-immuno-PET for imaging of long circulating drugs and disease targets: why, how and when to be applied?. Quarterly Journal of Nuclear Medicine and Molecular Imaging, 2015, 59, 18-38.	0.7	38
172	Image derived input functions for dynamic High Resolution Research Tomograph PET brain studies. NeuroImage, 2008, 43, 676-686.	4.2	37
173	Amyloid and its association with default network integrity in Alzheimer's disease. Human Brain Mapping, 2014, 35, 779-791.	3.6	37
174	Quantitative implications of the updated EARL 2019 PET–CT performance standards. EJNMMI Physics, 2019, 6, 28.	2.7	37
175	A systematic review and quality of reporting checklist for repeatability and reproducibility of radiomic features. Physics and Imaging in Radiation Oncology, 2021, 20, 69-75.	2.9	37
176	Kinetic analysis in human brain of [11C](R)-rolipram, a positron emission tomographic radioligand to image phosphodiesterase 4: A retest study and use of an image-derived input function. NeuroImage, 2011, 54, 1903-1909.	4.2	36
177	Impact of partial-volume correction in oncological PET studies: a systematic review and meta-analysis. European Journal of Nuclear Medicine and Molecular Imaging, 2017, 44, 2105-2116.	6.4	36
178	Quantitative PET in the 2020s: a roadmap. Physics in Medicine and Biology, 2021, 66, 06RM01.	3.0	36
179	Prognostic Impact of [18F]Fluorothymidine and [18F]Fluoro-D-Glucose Baseline Uptakes in Patients with Lung Cancer Treated First-Line with Erlotinib. PLoS ONE, 2013, 8, e53081.	2.5	36
180	Correction methods for missing data in sinograms of the HRRT PET scanner. IEEE Transactions on Nuclear Science, 2003, 50, 1452-1456.	2.0	34

#	Article	IF	CITATIONS
181	Quantification of Dopamine Transporter Binding Using [18F]FP-β-CIT and Positron Emission Tomography. Journal of Cerebral Blood Flow and Metabolism, 2007, 27, 1397-1406.	4.3	34
182	Comparison of 3D-OP-OSEM and 3D-FBP reconstruction algorithms for High-Resolution Research Tomograph studies: effects of randoms estimation methods. Physics in Medicine and Biology, 2008, 53, 3217-3230.	3.0	34
183	Quantitative comparison of analytic and iterative reconstruction methods in 2- and 3-dimensional dynamic cardiac 18F-FDG PET. Journal of Nuclear Medicine, 2004, 45, 2008-15.	5.0	34
184	Dual-Phase PET-CT to Differentiate [18F]Fluoromethylcholine Uptake in Reactive and Malignant Lymph Nodes in Patients with Prostate Cancer. PLoS ONE, 2012, 7, e48430.	2.5	33
185	Relative cerebral flow from dynamic PIB scans as an alternative for FDG scans in Alzheimer's disease PET studies. PLoS ONE, 2019, 14, e0211000.	2.5	33
186	Multiparametric functional MRI and 18F-FDG-PET for survival prediction in patients with head and neck squamous cell carcinoma treated with (chemo)radiation. European Radiology, 2021, 31, 616-628.	4.5	33
187	Evaluation of Methods for Generating Parametric (R)-[11C]PK11195 Binding Images. Journal of Cerebral Blood Flow and Metabolism, 2007, 27, 1603-1615.	4.3	32
188	Quantification of <sup>18</sup> F-Fluorocholine Kinetics in Patients with Prostate Cancer. Journal of Nuclear Medicine, 2015, 56, 365-371.	5.0	32
189	Lungtech, a phase II EORTC trial of SBRT for centrally located lung tumours – a clinical physics perspective. Radiation Oncology, 2016, 11, 7.	2.7	32
190	Does PET Reconstruction Method Affect Deauville Scoring in Lymphoma Patients?. Journal of Nuclear Medicine, 2018, 59, 1167-1169.	5.0	32
191	Simplified Methods for Quantification of <sup>18</sup> F-DCFPyL Uptake in Patients with Prostate Cancer. Journal of Nuclear Medicine, 2019, 60, 1730-1735.	5.0	32
192	Optimizing Workflows for Fast and Reliable Metabolic Tumor Volume Measurements in Diffuse Large B Cell Lymphoma. Molecular Imaging and Biology, 2020, 22, 1102-1110.	2.6	32
193	Advanced analytics and artificial intelligence in gastrointestinal cancer: a systematic review of radiomics predicting response to treatment. European Journal of Nuclear Medicine and Molecular Imaging, 2021, 48, 1785-1794.	6.4	32
194	Hyperaemic microvascular resistance is not increased in viable myocardium after chronic myocardial infarction. European Heart Journal, 2007, 28, 2320-2325.	2.2	30
195	Impact of <scp>PET</scp> / <scp>CT</scp> system, reconstruction protocol, data analysis method, and repositioning on <scp>PET</scp> / <scp>CT</scp> precision: An experimental evaluation using an oncology and brain phantom. Medical Physics, 2017, 44, 6413-6424.	3.0	30
196	Matching PET and CT scans of the head and neck area: Development of method and validation. Medical Physics, 2002, 29, 2230-2238.	3.0	29
197	PPET: A software tool for kinetic and parametric analyses of dynamic PET studies. NeuroImage, 2006, 31, T62.	4.2	29
198	Downregulation of <sup>18</sup> F-FDG Uptake in PET as an Early Pharmacodynamic Effect in Treatment of Non–Small Cell Lung Cancer with the mTOR Inhibitor Everolimus. Journal of Nuclear Medicine, 2009, 50, 1815-1819.	5.0	29

#	Article	IF	CITATIONS
199	Quantification of (R)-[11C]PK11195 binding in rheumatoid arthritis. European Journal of Nuclear Medicine and Molecular Imaging, 2009, 36, 624-631.	6.4	29
200	Off-line motion correction methods for multi-frame PET data. European Journal of Nuclear Medicine and Molecular Imaging, 2009, 36, 2002-2013.	6.4	29
201	Regional [18F]flortaucipir PET is more closely associated with disease severity than CSF p-tau in Alzheimer's disease. European Journal of Nuclear Medicine and Molecular Imaging, 2020, 47, 2866-2878.	6.4	29
202	Predictive value of quantitative 18F-FDG-PET radiomics analysis in patients with head and neck squamous cell carcinoma. EJNMMI Research, 2020, 10, 102.	2.5	29
203	Microvascular Function in Viable Myocardium After Chronic Infarction Does Not Influence Fractional Flow Reserve Measurements. Journal of Nuclear Medicine, 2007, 48, 1987-1992.	5.0	28
204	<i>In vivo</i> Validation of Reconstruction-Based Resolution Recovery for Human Brain Studies. Journal of Cerebral Blood Flow and Metabolism, 2010, 30, 381-389.	4.3	28
205	Bias Reduction for Low-Statistics PET: Maximum Likelihood Reconstruction With a Modified Poisson Distribution. IEEE Transactions on Medical Imaging, 2015, 34, 126-136.	8.9	28
206	Accuracy and Precision of Partial-Volume Correction in Oncological PET/CT Studies. Journal of Nuclear Medicine, 2016, 57, 1642-1649.	5.0	28
207	Tau pathology and relative cerebral blood flow are independently associated with cognition in Alzheimer's disease. European Journal of Nuclear Medicine and Molecular Imaging, 2020, 47, 3165-3175.	6.4	28
208	SPM analysis of parametric (R)-[11C]PK11195 binding images: Plasma input versus reference tissue parametric methods. NeuroImage, 2007, 35, 1473-1479.	4.2	26
209	Impact of attenuation correction strategies on the quantification of High Resolution Research Tomograph PET studies. Physics in Medicine and Biology, 2008, 53, 99-118.	3.0	26
210	Repeatability of [18F]FDG PET/CT total metabolic active tumour volume and total tumour burden in NSCLC patients. EJNMMI Research, 2019, 9, 14.	2.5	26
211	Multicenter <scp>CT</scp> phantoms public dataset for radiomics reproducibility tests. Medical Physics, 2019, 46, 1512-1518.	3.0	26
212	Detection of prostate cancer with 18F-DCFPyL PET/CT compared to final histopathology of radical prostatectomy specimens: is PSMA-targeted biopsy feasible? The DeTeCT trial. World Journal of Urology, 2021, 39, 2439-2446.	2.2	26
213	Functional stress imaging to predict abnormal coronary fractional flow reserve: the PACIFIC 2 study. European Heart Journal, 2022, 43, 3118-3128.	2.2	26
214	Retrospective quality control review of FDG scans in the imaging sub-study of PALETTE EORTC 62072/VEG110727: a randomized, double-blind, placebo-controlled phase III trial. European Journal of Nuclear Medicine and Molecular Imaging, 2015, 42, 848-857.	6.4	25
215	Quantification of subendocardial and subepicardial blood flow using 15O-labeled water and PET: experimental validation. Journal of Nuclear Medicine, 2006, 47, 163-72.	5.0	25
216	Gap Filling Strategies for 3-D-FBP Reconstructions of High-Resolution Research Tomograph Scans. IEEE Transactions on Medical Imaging, 2008, 27, 934-942.	8.9	24

#	Article	IF	CITATIONS
217	Reference Tissue Models and Blood–Brain Barrier Disruption: Lessons from ( <i>R</i> )-[ <sup>11</sup> C]PK11195 in Traumatic Brain Injury. Journal of Nuclear Medicine, 2009, 50, 1975-1979.	5.0	24
218	Measurement of metabolic tumor volume: static versus dynamic FDG scans. EJNMMI Research, 2011, 1, 35.	2.5	24
219	Standardization of Quantitative Imaging: The Time Is Right, and 18F-FDG PET/CT Is a Good Place to Start. Journal of Nuclear Medicine, 2011, 52, 171-172.	5.0	24
220	Comparison of Simplified Parametric Methods for Visual Interpretation of <sup>11</sup> C-Pittsburgh Compound-B PET Images. Journal of Nuclear Medicine, 2014, 55, 1305-1307.	5.0	24
221	<sup>18</sup> F-FDG or 3â€2-Deoxy-3â€2- <sup>18</sup> F-Fluorothymidine to Detect Transformation of Follicular Lymphoma. Journal of Nuclear Medicine, 2015, 56, 216-221.	5.0	24
222	Comparison of Velocity- and Acceleration-Selective Arterial Spin Labeling with [ <sup>15</sup> 0]H <sub>2</sub> 0 Positron Emission Tomography. Journal of Cerebral Blood Flow and Metabolism, 2015, 35, 1296-1303.	4.3	24
223	PET Tracers for Imaging of ABC Transporters at the Blood-Brain Barrier: Principles and Strategies. Current Pharmaceutical Design, 2016, 22, 5779-5785.	1.9	24
224	Delayed contrast enhancement and perfusable tissue index in hypertrophic cardiomyopathy: comparison between cardiac MRI and PET. Journal of Nuclear Medicine, 2005, 46, 923-9.	5.0	24
225	Pharmacokinetic analysis of [18F]FAZA in non-small cell lung cancer patients. European Journal of Nuclear Medicine and Molecular Imaging, 2013, 40, 1523-1531.	6.4	23
226	Metabolic activity measured by FDG PET predicts pathological response in locally advanced superior sulcus NSCLC. Lung Cancer, 2014, 85, 205-212.	2.0	23
227	Interaction of quantitative <sup>18</sup> Fâ€FDGâ€PETâ€CT imaging parameters and human papillomavirus status in oropharyngeal squamous cell carcinoma. Head and Neck, 2016, 38, 529-535.	2.0	23
228	Parametric Binding Images of the TSPO Ligand <sup>18</sup> F-DPA-714. Journal of Nuclear Medicine, 2016, 57, 1543-1547.	5.0	23
229	Textural features of 18F-fluorodeoxyglucose positron emission tomography scanning in diagnosing aortic prosthetic graft infection. European Journal of Nuclear Medicine and Molecular Imaging, 2017, 44, 886-894.	6.4	23
230	Healthy Tissue Uptake of 68Ga-Prostate-Specific Membrane Antigen, 18F-DCFPyL, 18F-Fluoromethylcholine, and 18F-Dihydrotestosterone. Journal of Nuclear Medicine, 2019, 60, 1111-1117.	5.0	23
231	Test–retest repeatability of [ <sup>18</sup> F]Flortaucipir PET in Alzheimer's disease and cognitively normal individuals. Journal of Cerebral Blood Flow and Metabolism, 2020, 40, 2464-2474.	4.3	23
232	Quantitative and Simplified Analysis of <sup>11</sup> C-Erlotinib Studies. Journal of Nuclear Medicine, 2016, 57, 861-866.	5.0	22
233	Repeatability of Quantitative <sup>18</sup> F-Fluoromethylcholine PET/CT Studies in Prostate Cancer. Journal of Nuclear Medicine, 2016, 57, 721-727.	5.0	22
234	Quantification of [ <sup>18</sup> F]florbetapir: A test–retest tracer kinetic modelling study. Journal of Cerebral Blood Flow and Metabolism, 2019, 39, 2172-2180.	4.3	22

#	Article	IF	CITATIONS
235	Radiomics in Vulvar Cancer: First Clinical Experience Using <sup>18</sup> F-FDG PET/CT Images. Journal of Nuclear Medicine, 2019, 60, 199-206.	5.0	22
236	Parametric methods for [ <sup>18</sup> F]flortaucipir PET. Journal of Cerebral Blood Flow and Metabolism, 2020, 40, 365-373.	4.3	22
237	[89Zr]Zr-cetuximab PET/CT as biomarker for cetuximab monotherapy in patients with RAS wild-type advanced colorectal cancer. European Journal of Nuclear Medicine and Molecular Imaging, 2020, 47, 849-859.	6.4	22
238	Repeatability of Quantitative <sup>18</sup> F-DCFPyL PET/CT Measurements in Metastatic Prostate Cancer. Journal of Nuclear Medicine, 2020, 61, 1320-1325.	5.0	22
239	Harmonisation of PET/CT contrast recovery performance for brain studies. European Journal of Nuclear Medicine and Molecular Imaging, 2021, 48, 2856-2870.	6.4	22
240	The perfusable tissue index: a marker of myocardial viability. Journal of Nuclear Cardiology, 2003, 10, 684-691.	2.1	21
241	Experimental evaluation of iterative reconstruction versus filtered back projection for 3D [150]water PET activation studies using statistical parametric mapping analysis. Neurolmage, 2003, 19, 1170-1179.	4.2	21
242	Attenuation correction of PET activation studies in the presenceof task-related motion. NeuroImage, 2003, 19, 1501-1509.	4.2	21
243	Test-Retest Variability of Various Quantitative Measures to Characterize Tracer Uptake and/or Tracer Uptake Heterogeneity in Metastasized Liver for Patients with Colorectal Carcinoma. Molecular Imaging and Biology, 2014, 16, 13-18.	2.6	21
244	Preclinical evaluation of [18F]PK-209, a new PET ligand for imaging the ion-channel site of NMDA receptors. Nuclear Medicine and Biology, 2015, 42, 205-212.	0.6	21
245	Partial volume correction of brain PET studies using iterative deconvolution in combination with HYPR denoising. EJNMMI Research, 2017, 7, 36.	2.5	21
246	PET and CSF amyloid-β status are differently predicted by patient features: information from discordant cases. Alzheimer's Research and Therapy, 2019, 11, 100.	6.2	21
247	Evaluation of Tracer Kinetic Models for Analysis of [18F]FDDNP Studies. Molecular Imaging and Biology, 2009, 11, 322-333.	2.6	20
248	[18F]FDG PET/CT-based response assessment of stage IV non-small cell lung cancer treated with paclitaxel-carboplatin-bevacizumab with or without nitroglycerin patches. European Journal of Nuclear Medicine and Molecular Imaging, 2017, 44, 8-16.	6.4	20
249	Visceral adipose tissue volume is associated with premature atherosclerosis in early type 2 diabetes mellitus independent of traditional risk factors. Atherosclerosis, 2019, 290, 87-93.	0.8	20
250	The Impact of Semiautomatic Segmentation Methods on Metabolic Tumor Volume, Intensity, and Dissemination Radiomics in <sup>18</sup> F-FDG PET Scans of Patients with Classical Hodgkin Lymphoma. Journal of Nuclear Medicine, 2022, 63, 1424-1430.	5.0	20
251	Measurement of left ventricular volumes and function with O-15–labeled carbon monoxide gated positron emission tomography: Comparison with magnetic resonance imaging. Journal of Nuclear Cardiology, 2005, 12, 639-644.	2.1	19
252	Accurate Delineation of Glioma Infiltration by Advanced PET/MR Neuro-Imaging (FRONTIER Study). Neurosurgery, 2016, 79, 535-540.	1.1	19

#	Article	IF	CITATIONS
253	Quantification of the novel <i>N</i> -methyl- <scp>d</scp> -aspartate receptor ligand [ <sup>11</sup> C]GMOM in man. Journal of Cerebral Blood Flow and Metabolism, 2016, 36, 1111-1121.	4.3	19
254	In Vivo Evaluation of <sup>11</sup> C-Preladenant for PET Imaging of Adenosine A <sub>2A</sub> Receptors in the Conscious Monkey. Journal of Nuclear Medicine, 2017, 58, 762-767.	5.0	19
255	Incorporating HYPR de-noising within iterative PET reconstruction (HYPR-OSEM). Physics in Medicine and Biology, 2017, 62, 6666-6687.	3.0	19
256	Prognostic value of total lesion glycolysis and metabolic active tumor volume in non-small cell lung cancer. Cancer Treatment and Research Communications, 2018, 15, 7-12.	1.7	19
257	A novel partial volume correction method for accurate quantification of [18F] flortaucipir in the hippocampus. EJNMMI Research, 2018, 8, 79.	2.5	19
258	Diagnostic performance of regional cerebral blood flow images derived from dynamic PIB scans in Alzheimer's disease. EJNMMI Research, 2019, 9, 59.	2.5	19
259	Metabolic Biomarker–Based BRAFV600 Mutation Association and Prediction in Melanoma. Journal of Nuclear Medicine, 2019, 60, 1545-1552.	5.0	19
260	Spatial concordance of DNA methylation classification in diffuse glioma. Neuro-Oncology, 2021, 23, 2054-2065.	1.2	19
261	Repeatability of IVIM biomarkers from diffusionâ€weighted MRI in head and neck: Bayesian probability versus neural network. Magnetic Resonance in Medicine, 2021, 85, 3394-3402.	3.0	19
262	Methodological Aspects of Multicenter Studies with Quantitative PET. Methods in Molecular Biology, 2011, 727, 335-349.	0.9	19
263	Repeatability of arterial input functions and kinetic parameters in muscle obtained by dynamic contrast enhanced MR imaging of the head and neck. Magnetic Resonance Imaging, 2020, 68, 1-8.	1.8	19
264	Pemetrexed Induced Thymidylate Synthase Inhibition in Non-Small Cell Lung Cancer Patients: A Pilot Study with 3′-Deoxy-3′-[18F]fluorothymidine Positron Emission Tomography. PLoS ONE, 2013, 8, e63705.	2.5	19
265	Interim positron emission tomography scan in multi-center studies: optimization of visual and quantitative assessments. Leukemia and Lymphoma, 2009, 50, 1748-1749.	1.3	18
266	No Evidence for Additional Blood–Brain Barrier P-Glycoprotein Dysfunction in Alzheimer's Disease Patients with Microbleeds. Journal of Cerebral Blood Flow and Metabolism, 2012, 32, 1468-1471.	4.3	18
267	The Association of Glucose Metabolism and Eigenvector Centrality in Alzheimer's Disease. Brain Connectivity, 2016, 6, 1-8.	1.7	18
268	Model selection criteria for dynamic brain PET studies. EJNMMI Physics, 2017, 4, 30.	2.7	18
269	Mapping heterogeneity in glucose uptake in metastatic melanoma using quantitative 18F-FDG PET/CT analysis. EJNMMI Research, 2018, 8, 101.	2.5	18
270	Feasibility of PET/CT system performance harmonisation for quantitative multicentre 89Zr studies. EJNMMI Physics, 2018, 5, 26.	2.7	18

#	Article	IF	CITATIONS
271	Recovery of myocardial perfusion after percutaneous coronary intervention of chronic total occlusions is comparable to hemodynamically significant nonâ€occlusive lesions. Catheterization and Cardiovascular Interventions, 2019, 93, 1059-1066.	1.7	18
272	COVID-19 and the brain: impact on nuclear medicine in neurology. European Journal of Nuclear Medicine and Molecular Imaging, 2020, 47, 2487-2492.	6.4	18
273	Arterial wall inflammation is increased in rheumatoid arthritis compared with osteoarthritis, as a marker of early atherosclerosis. Rheumatology, 2021, 60, 3360-3368.	1.9	18
274	Baseline and interim PETâ€based outcome prediction in peripheral Tâ€cell lymphoma: A subgroup analysis of the PETAL trial. Hematological Oncology, 2020, 38, 244-256.	1.7	18
275	Influence of ROI definition, partial volume correction and SUV normalization on SUV–survival correlation in oesophageal cancer. Nuclear Medicine Communications, 2010, 31, 652-658.	1.1	18
276	Ischaemic burden and changes in absolute myocardial perfusion after chronic total occlusion percutaneous coronary intervention. EuroIntervention, 2020, 16, e462-e471.	3.2	18
277	Assessment of Simplified Methods to Measure <sup>18</sup> F-FLT Uptake Changes in EGFR-Mutated Non–Small Cell Lung Cancer Patients Undergoing EGFR Tyrosine Kinase Inhibitor Treatment. Journal of Nuclear Medicine, 2014, 55, 1417-1423.	5.0	17
278	Quantification of Dynamic <sup>11</sup> C-Phenytoin PET Studies. Journal of Nuclear Medicine, 2015, 56, 1372-1377.	5.0	17
279	Guidelines for quality control of PET/CT scans in a multicenter clinical study. EJNMMI Physics, 2017, 4, 23.	2.7	17
280	PET segmentation of bulky tumors: Strategies and workflows to improve inter-observer variability. PLoS ONE, 2020, 15, e0230901.	2.5	17
281	Use of population input functions for reduced scan duration whole-body Patlak 18F-FDG PET imaging. EJNMMI Physics, 2021, 8, 11.	2.7	17
282	Validation of a multiwell gamma-counter for measuring high-pressure liquid chromatography metabolite profiles. Journal of Nuclear Medicine Technology, 2004, 32, 28-32.	0.8	17
283	Limbic and motor circuits involved in symmetry behavior in Tourette's syndrome. CNS Spectrums, 2013, 18, 34-42.	1.2	16
284	Challenges of quantification of TSPO in the human brain. Clinical and Translational Imaging, 2015, 3, 403-416.	2.1	16
285	A new perspective for advanced positron emission tomography–based molecular imaging in neurodegenerative proteinopathies. Alzheimer's and Dementia, 2019, 15, 1081-1103.	0.8	16
286	Variability and Repeatability of Quantitative Uptake Metrics in <sup>18</sup> F-FDG PET/CT of Non–Small Cell Lung Cancer: Impact of Segmentation Method, Uptake Interval, and Reconstruction Protocol. Journal of Nuclear Medicine, 2019, 60, 600-607.	5.0	16
287	Classification of negative and positive 18F-florbetapir brain PET studies in subjective cognitive decline patients using a convolutional neural network. European Journal of Nuclear Medicine and Molecular Imaging, 2021, 48, 721-728.	6.4	16
288	[ <sup>18</sup> F]Flortaucipir PET Across Various <i>MAPT</i> Mutations in Presymptomatic and Symptomatic Carriers. Neurology, 2021, 97, e1017-e1030.	1.1	16

#	Article	IF	CITATIONS
289	Quantitative Radiomics Features in Diffuse Large B-Cell Lymphoma: Does Segmentation Method Matter?. Journal of Nuclear Medicine, 2022, 63, 389-395.	5.0	16
290	Measurement of 18F-FDG concentrations in blood samples: comparison of direct calibration and standard solution methods. Journal of Nuclear Medicine Technology, 2003, 31, 206-9.	0.8	16
291	Myocardial Oxygen Extraction Fraction Measured Using Bolus Inhalation of <sup>15</sup> O-Oxygen Gas and Dynamic PET. Journal of Nuclear Medicine, 2011, 52, 60-66.	5.0	15
292	Optimization of parathyroid 11C-choline PET protocol for localization of parathyroid adenomas in patients with primary hyperparathyroidism. EJNMMI Research, 2019, 9, 73.	2.5	15
293	Plausibility and redundancy analysis to select FDGâ€PET textural features in nonâ€small cell lung cancer. Medical Physics, 2021, 48, 1226-1238.	3.0	15
294	Dynamic PET image reconstruction utilizing intrinsic dataâ€driven HYPR4D denoising kernel. Medical Physics, 2021, 48, 2230-2244.	3.0	15
295	Repeatability of two semi-automatic artificial intelligence approaches for tumor segmentation in PET. EJNMMI Research, 2021, 11, 4.	2.5	15
296	Multicentre quantitative 68Ga PET/CT performance harmonisation. EJNMMI Physics, 2019, 6, 19.	2.7	15
297	Targeting PSMA Revolutionizes the Role of Nuclear Medicine in Diagnosis and Treatment of Prostate Cancer. Cancers, 2022, 14, 1169.	3.7	15
298	Quantification of O-(2-[18F]fluoroethyl)-L-tyrosine kinetics in glioma. EJNMMI Research, 2018, 8, 72.	2.5	14
299	SMART (SiMulAtion and ReconsTruction) PET: an efficient PET simulation-reconstruction tool. EJNMMI Physics, 2018, 5, 16.	2.7	14
300	3′-Deoxy-3′-[18F]Fluorothymidine Positron Emission Tomography Depicts Heterogeneous Proliferation Pathology in Idiopathic Pulmonary Arterial Hypertension Patient Lung. Circulation: Cardiovascular Imaging, 2018, 11, e007402.	2.6	14
301	Pharmacokinetic Modeling of [18F]MC225 for Quantification of the P-Glycoprotein Function at the Blood–Brain Barrier in Non-Human Primates with PET. Molecular Pharmaceutics, 2020, 17, 3477-3486.	4.6	14
302	Tau PET and relative cerebral blood flow in dementia with Lewy bodies: A PET study. NeuroImage: Clinical, 2020, 28, 102504.	2.7	14
303	Kinetics and 28-day test–retest repeatability and reproducibility of [ <sup>11</sup> C]UCB-J PET brain imaging. Journal of Cerebral Blood Flow and Metabolism, 2021, 41, 1338-1350.	4.3	14
304	Strategies to reduce sample sizes in Alzheimer's disease primary and secondary prevention trials using longitudinal amyloid PET imaging. Alzheimer's Research and Therapy, 2021, 13, 82.	6.2	14
305	Bone Metastases Are Measurable: The Role of Whole-Body MRI and Positron Emission Tomography. Frontiers in Oncology, 2021, 11, 772530.	2.8	14
306	Early Response Prediction of Multiparametric Functional MRI and 18F-FDG-PET in Patients with Head and Neck Squamous Cell Carcinoma Treated with (Chemo)Radiation. Cancers, 2022, 14, 216.	3.7	14

#	Article	IF	CITATIONS
307	Impact of Scar on Water-Perfusable Tissue Index in Chronic Ischemic Heart Disease. Molecular Imaging and Biology, 2006, 8, 245-251.	2.6	13
308	NEOadjuvant therapy monitoring with PET and CT in Esophageal Cancer (NEOPEC-trial). BMC Medical Physics, 2008, 8, 3.	2.4	13
309	Performance of a modified supervised cluster algorithm for extracting reference region input functions from (R)-[ <sup>11</sup> C]PK11195 brain PET studies. , 2008, , .		13
310	Comparison of transcranial Doppler ultrasonography and positron emission tomography using a three-dimensional template of the middle cerebral artery. Neurological Research, 2009, 31, 52-59.	1.3	13
311	Effects of rigid and non-rigid image registration on test-retest variability of quantitative [18F]FDG PET/CT studies. EJNMMI Research, 2012, 2, 10.	2.5	13
312	Comparison of HRRT and HR+ Scanners for Quantitative (R)-[11C]verapamil, [11C]raclopride and [11C]flumazenil Brain Studies. Molecular Imaging and Biology, 2015, 17, 129-139.	2.6	13
313	Pharmacokinetic modeling of a novel hypoxia PET tracer [18F]HX4 in patients with non-small cell lung cancer. EJNMMI Physics, 2016, 3, 30.	2.7	13
314	Multiparametric Analysis of the Relationship Between Tumor Hypoxia and Perfusion with <sup>18</sup> F-Fluoroazomycin Arabinoside and <sup>15</sup> O-H <sub>2</sub> O PET. Journal of Nuclear Medicine, 2016, 57, 530-535.	5.0	13
315	Variability in quantitative analysis of atherosclerotic plaque inflammation using 18F-FDG PET/CT. PLoS ONE, 2017, 12, e0181847.	2.5	13
316	Noise-Induced Variability of Immuno-PET with Zirconium-89-Labeled Antibodies: an Analysis Based on Count-Reduced Clinical Images. Molecular Imaging and Biology, 2018, 20, 1025-1034.	2.6	13
317	Factors affecting the harmonization of diseaseâ€related metabolic brain pattern expression quantification in [ <sup>18</sup> F]FDGâ€PET (PETMETPAT). Alzheimer's and Dementia: Diagnosis, Assessment and Disease Monitoring, 2019, 11, 472-482.	2.4	13
318	Task Group 174 Report: Utilization of [ 18 F]Fluorodeoxyglucose Positron Emission Tomography ([ 18) Tj ETQq	0 0 0 rgBT	/Overlock 10
319	Comparison Between the Performance of Quantitative Flow Ratio and PerfusionÂlmaging for Diagnosing Myocardial Ischemia. JACC: Cardiovascular Imaging, 2020, 13, 1976-1985.	5.3	13
320	Moving the goalposts while scoring―the dilemma posed by new PET technologies. European Journal of Nuclear Medicine and Molecular Imaging, 2021, 48, 2696-2710.	6.4	13
321	Crossed Cerebellar Diaschisis in Alzheimer's Disease. Current Alzheimer Research, 2018, 15, 1267-1275.	1.4	13
322	Effects of attenuation correction and reconstruction method on PET activation studies. Neurolmage, 2003, 20, 898-908.	4.2	12
323	Optimization of attenuation correction for positron emission tomography studies of thorax and pelvis using count-based transmission scans. Physics in Medicine and Biology, 2004, 49, N31-N38.	3.0	12
324	Image Derived Input Functions: Effects of Motion on Tracer Kinetic Analyses. Molecular Imaging and Biology, 2011, 13, 25-31.	2.6	12

#	Article	IF	CITATIONS
325	Parametric Methods for Quantification of 18F-FAZA Kinetics in Non–Small Cell Lung Cancer Patients. Journal of Nuclear Medicine, 2014, 55, 1772-1777.	5.0	12
326	Vemurafenib plus cobimetinib in unresectable stage IIIc or stage IV melanoma: response monitoring and resistance prediction with positron emission tomography and tumor characteristics (REPOSIT): study protocol of a phase II, open-label, multicenter study. BMC Cancer, 2017, 17, 649.	2.6	12
327	<sup>18</sup> F-FDG-PET uptake in non-infected total hip prostheses. Monthly Notices of the Royal Astronomical Society: Letters, 2018, 89, 634-639.	3.3	12
328	Partial-volume correction in dynamic PET-CT: effect on tumor kinetic parameter estimation and validation of simplified metrics. EJNMMI Research, 2019, 9, 12.	2.5	12
329	Clinically Valuable Quality Control for PET/MRI Systems: Consensus Recommendation From the HYBRID Consortium. Frontiers in Physics, 2019, 7, .	2.1	12
330	Semi-quantitative cerebral blood flow parameters derived from non-invasive [ <sup>15</sup> 0]H <sub>2</sub> 0 PET studies. Journal of Cerebral Blood Flow and Metabolism, 2019, 39, 163-172.	4.3	12
331	Simulating the effect of cerebral blood flow changes on regional quantification of [ <sup>18</sup> F]flutemetamol and [ <sup>18</sup> F]florbetaben studies. Journal of Cerebral Blood Flow and Metabolism, 2021, 41, 579-589.	4.3	12
332	<sup>18</sup> F-FDG PET Improves Baseline Clinical Predictors of Response in Diffuse Large B-Cell Lymphoma: The HOVON-84 Study. Journal of Nuclear Medicine, 2022, 63, 1001-1007.	5.0	12
333	Postinjection transmission scanning in myocardial 18F-FDG PET studies using both filtered backprojection and iterative reconstruction. Journal of Nuclear Medicine, 2004, 45, 169-75.	5.0	12
334	Quantitative Experimental Comparison of HRRT versus HR+ PET Brain Studies. , 2006, , .		11
335	Imaging trauma in vivo: GABAA benzodiazepine receptor binding. Molecular Psychiatry, 2008, 13, 3-3.	7.9	11
336	Validation of simplified dosimetry approaches in 89 Zr-PET/CT: The use of manual versus semi-automatic delineation methods to estimate organ absorbed doses. Medical Physics, 2014, 41, 102503.	3.0	11
337	Investigation of practical initial attenuation image estimates in TOFâ€MLAA reconstruction for PET/MR. Medical Physics, 2016, 43, 4163-4173.	3.0	11
338	Quality assessment of positron emission tomography scans: recommendations for future multicentre trials. Acta Oncológica, 2017, 56, 1459-1464.	1.8	11
339	Repeatability of quantitative 18F-FLT uptake measurements in solid tumors: an individual patient data multi-center meta-analysis. European Journal of Nuclear Medicine and Molecular Imaging, 2018, 45, 951-961.	6.4	11
340	Prognostic Value of [ 18 F]-Fluoromethylcholine Positron Emission Tomography/Computed Tomography Before Stereotactic Body Radiation Therapy for Oligometastatic Prostate Cancer. International Journal of Radiation Oncology Biology Physics, 2018, 101, 406-410.	0.8	11
341	Impact of Specific Crossing Techniques in Chronic Total Occlusion Percutaneous Coronary Intervention on Recovery of Absolute Myocardial Perfusion. Circulation: Cardiovascular Interventions, 2019, 12, e008064.	3.9	11
342	Interobserver reproducibility of tumor uptake quantification with 89Zr-immuno-PET: a multicenter analysis. European Journal of Nuclear Medicine and Molecular Imaging, 2019, 46, 1840-1849.	6.4	11

#	Article	IF	CITATIONS
343	Influence of ROI definition, partial volume correction and SUV normalization on SUV-survival correlation in oesophageal cancer. Nuclear Medicine Communications, 2010, 31, 652-8.	1.1	11
344	First-time imaging of [89Zr]trastuzumab in breast cancer using a long axial field-of-view PET/CT scanner. European Journal of Nuclear Medicine and Molecular Imaging, 2022, 49, 3593-3595.	6.4	11
345	Maximum-likelihood reconstruction based on a modified Poisson distribution to reduce bias in PET. , 2011, , .		10
346	A Clinical and Experimental Comparison of Time of Flight PET/MRI and PET/CT Systems. Molecular Imaging and Biology, 2015, 17, 714-725.	2.6	10
347	Quantitative agreement between [ <sup>15</sup> 0]H <sub>2</sub> 0 PET and model free QUASAR MRIâ€derived cerebral blood flow and arterial blood volume. NMR in Biomedicine, 2016, 29, 519-526.	2.8	10
348	Sensitivity of 18F-fluorodihydrotestosterone PET-CT to count statistics and reconstruction protocol in metastatic castration-resistant prostate cancer. EJNMMI Research, 2019, 9, 70.	2.5	10
349	Quantitative assessment of 18F-FDG PET in patients with Hodgkin lymphoma. Nuclear Medicine Communications, 2019, 40, 249-257.	1.1	10
350	Lesion Detection and Interobserver Agreement with Advanced Image Reconstruction for <sup>18</sup> F-DCFPyL PET/CT in Patients with Biochemically Recurrent Prostate Cancer. Journal of Nuclear Medicine, 2020, 61, 210-216.	5.0	10
351	The Additional Value of Ultrafast DCE-MRI to DWI-MRI and 18F-FDG-PET to Detect Occult Primary Head and Neck Squamous Cell Carcinoma. Cancers, 2020, 12, 2826.	3.7	10
352	Repeatability of parametric methods for [ <sup>18</sup> F]florbetapir imaging in Alzheimer's disease and healthy controls: A test–retest study. Journal of Cerebral Blood Flow and Metabolism, 2021, 41, 569-578.	4.3	10
353	Adherence to pretreatment and intratreatment imaging of head and neck squamous cell carcinoma patients undergoing (chemo) radiotherapy in a research setting. Clinical Imaging, 2021, 69, 82-90.	1.5	10
354	Effect of Shortening the Scan Duration on Quantitative Accuracy of [18F]Flortaucipir Studies. Molecular Imaging and Biology, 2021, 23, 604-613.	2.6	10
355	Positron emission tomography to assess hypoxia and perfusion in lung cancer. World Journal of Clinical Oncology, 2014, 5, 824.	2.3	10
356	Diagnostic Performance of [18F]FDG PET in Staging Grade 1–2, Estrogen Receptor Positive Breast Cancer. Diagnostics, 2021, 11, 1954.	2.6	10
357	Correction for emission contamination in transmission scans for the high resolution research tomograph. IEEE Transactions on Nuclear Science, 2004, 51, 673-676.	2.0	9
358	Hemodynamic changes in ipsi- and contralateral cerebral arterial territories after carotid endarterectomy using positron emission tomography. World Neurosurgery, 2009, 71, 668-676.	1.3	9
359	Parametric [11C]flumazenil images. Nuclear Medicine Communications, 2012, 33, 422-430.	1.1	9
360	Optimisation and harmonisation: two sides of the same coin?. European Journal of Nuclear Medicine and Molecular Imaging, 2013, 40, 982-984.	6.4	9

#	Article	IF	CITATIONS
361	First in human evaluation of [18F]PK-209, a PET ligand for the ion channel binding site of NMDA receptors. EJNMMI Research, 2018, 8, 69.	2.5	9
362	Arterial wall inflammation in rheumatoid arthritis is reduced by anti-inflammatory treatment. Seminars in Arthritis and Rheumatism, 2021, 51, 457-463.	3.4	9
363	A dual-time-window protocol to reduce acquisition time of dynamic tau PET imaging using [18F]MK-6240. EJNMMI Research, 2021, 11, 49.	2.5	9
364	Influences on PET Quantification and Interpretation. Diagnostics, 2022, 12, 451.	2.6	9
365	First Evaluation of [11C]R116301 as an In Vivo Tracer of NK1 Receptors in Man. Molecular Imaging and Biology, 2009, 11, 241-245.	2.6	8
366	Comparison of oxygen-15 PET and transcranial Doppler CO2-reactivity measurements in identifying haemodynamic compromise in patients with symptomatic occlusion of the internal carotid artery. EJNMMI Research, 2012, 2, 30.	2.5	8
367	Methodological Considerations in Quantification of 3'-Deoxy-3'-[18F]Fluorothymidine Uptake Measured with Positron Emission Tomography in Patients with Non-Small Cell Lung Cancer. Molecular Imaging and Biology, 2014, 16, 136-145.	2.6	8
368	Translation of New Molecular Imaging Approaches to the Clinical Setting: Bridging the Gap to Implementation. Journal of Nuclear Medicine, 2016, 57, 96S-104S.	5.0	8
369	Altered GABA <sub>A</sub> receptor density and unaltered blood–brain barrier [ <sup>11</sup> C]flumazenil transport in drug-resistant epilepsy patients with mesial temporal sclerosis. Journal of Cerebral Blood Flow and Metabolism, 2017, 37, 97-105.	4.3	8
370	Subtle alterations in cerebrovascular reactivity in mild cognitive impairment detected by graph theoretical analysis and not by the standard approach. NeuroImage: Clinical, 2017, 15, 151-160.	2.7	8
371	Direct comparison of [11C] choline and [18F] FET PET to detect glioma infiltration: a diagnostic accuracy study in eight patients. EJNMMI Research, 2019, 9, 57.	2.5	8
372	Quantitative parametric maps of O-(2-[ <sup>18</sup> F]fluoroethyl)-L-tyrosine kinetics in diffuse glioma. Journal of Cerebral Blood Flow and Metabolism, 2020, 40, 895-903.	4.3	8
373	Why Is Amyloid-β PET Requested After Performing CSF Biomarkers?. Journal of Alzheimer's Disease, 2020, 73, 559-569.	2.6	8
374	[18F]FDG Uptake in Adipose Tissue Is Not Related to Inflammation in Type 2 Diabetes Mellitus. Molecular Imaging and Biology, 2021, 23, 117-126.	2.6	8
375	Interobserver Agreement on Automated Metabolic Tumor Volume Measurements of Deauville Score 4 and 5 Lesions at Interim <sup>18</sup> F-FDG PET in Diffuse Large B-Cell Lymphoma. Journal of Nuclear Medicine, 2021, 62, 1531-1536.	5.0	8
376	Differential associations between neocortical tau pathology and blood flow with cognitive deficits in early-onset vs late-onset Alzheimer's disease. European Journal of Nuclear Medicine and Molecular Imaging, 2022, 49, 1951-1963.	6.4	8
377	Simplified parametric methods for [18F]FDDNP studies. NeuroImage, 2010, 49, 433-441.	4.2	7
378	The effect of amyloid pathology and glucose metabolism on cortical volume loss over time in Alzheimer's disease. European Journal of Nuclear Medicine and Molecular Imaging, 2014, 41, 1190-8.	6.4	7

#	Article	IF	CITATIONS
379	Pharmacokinetic modeling of [11C]flumazenil kinetics in the rat brain. EJNMMI Research, 2017, 7, 17.	2.5	7
380	Episodic memory in mild cognitive impairment inversely correlates with the global modularity of the cerebral blood flow network. Psychiatry Research - Neuroimaging, 2018, 282, 73-81.	1.8	7
381	Optimization of the k2′ Parameter Estimation for the Pharmacokinetic Modeling of Dynamic PIB PET Scans Using SRTM2. Frontiers in Physics, 2019, 7, .	2.1	7
382	Letter to the Editor re: Semiquantitative Parameters in PSMA-Targeted PET Imaging with [18F]DCFPyL: Impact of Tumor Burden on Normal Organ Uptake. Molecular Imaging and Biology, 2020, 22, 15-17.	2.6	7
383	Evaluation of P-glycoprotein function at the blood–brain barrier using [18F]MC225-PET. European Journal of Nuclear Medicine and Molecular Imaging, 2021, 48, 4105-4106.	6.4	7
384	Updating PET/CT performance standards and PET/CT interpretation criteria should go hand in hand. EJNMMI Research, 2019, 9, 95.	2.5	7
385	Standardised uptake values as determined on prostateâ€specific membrane antigen positron emission tomography/computed tomography is associated with oncological outcomes in patients with prostate cancer. BJU International, 2022, 129, 768-776.	2.5	7
386	Prediction of Non-Response to Neoadjuvant Chemoradiotherapy in Esophageal Cancer Patients with 18F-FDG PET Radiomics Based Machine Learning Classification. Diagnostics, 2022, 12, 1070.	2.6	7
387	CTâ€perfusion versus [ <sup>15</sup> O]H <sub>2</sub> O PET in lung tumors: Effects of CTâ€perfusion methodology. Medical Physics, 2013, 40, 052502.	3.0	6
388	Evaluation of the Effect of Magnetic Field on PET Spatial Resolution and Contrast Recovery Using Clinical PET Scanners and EGSnrc Simulations. IEEE Transactions on Nuclear Science, 2015, 62, 101-110.	2.0	6
389	Wholeâ€body parametric PET imaging will replace conventional imageâ€derived PET metrics in clinical oncology. Medical Physics, 2018, 45, 5355-5358.	3.0	6
390	Tumour necrosis as assessed with 18F-FDG PET is a potential prognostic marker in diffuse large B cell lymphoma independent of MYC rearrangements. European Radiology, 2019, 29, 6018-6028.	4.5	6
391	In vivo tracking of single cells with PET. Nature Biomedical Engineering, 2020, 4, 765-766.	22.5	6
392	Head-to-head comparison of (R)-[11C]verapamil and [18F]MC225 in non-human primates, tracers for measuring P-glycoprotein function. European Journal of Nuclear Medicine and Molecular Imaging, 2021, 48, 4307-4317.	6.4	6
393	Performance of nanoScan PET/CT and PET/MR for quantitative imaging of 18F and 89Zr as compared with ex vivo biodistribution in tumor-bearing mice. EJNMMI Research, 2021, 11, 57.	2.5	6
394	The approval of a disease-modifying treatment for Alzheimer's disease: impact and consequences for the nuclear medicine community. European Journal of Nuclear Medicine and Molecular Imaging, 2021, 48, 3033-3036.	6.4	6
395	Potential and pitfalls of 89Zr-immuno-PET to assess target status: 89Zr-trastuzumab as an example. EJNMMI Research, 2021, 11, 74.	2.5	6
396	Effects of Tracer Uptake Time in Non–Small Cell Lung Cancer <sup>18</sup> F-FDG PET Radiomics. Journal of Nuclear Medicine, 2022, 63, 919-924.	5.0	6

#	Article	IF	CITATIONS
397	Use of an in-field-of-view shield to improve count rate performance of the single crystal layer high-resolution research tomograph PET scanner for small animal brain scans. Physics in Medicine and Biology, 2003, 48, N335-N342.	3.0	5
398	High Resolution PET Imaging Characteristics of /sup68/Ga, /sup124/I and /sup 89/Zr Compared to /sup 18/F. , 0, , .		5
399	Quantification of <sup>11</sup> C-Laniquidar Kinetics in the Brain. Journal of Nuclear Medicine, 2015, 56, 1730-1735.	5.0	5
400	Parametric Imaging of [11C]Flumazenil Binding in the Rat Brain. Molecular Imaging and Biology, 2018, 20, 114-123.	2.6	5
401	Primary tumor volume measurements in Ewing sarcoma: MRI inter- and intraobserver variability and comparison with FDG-PET. Acta Oncológica, 2018, 57, 534-540.	1.8	5
402	Exploring effects of Souvenaid on cerebral glucose metabolism in Alzheimer's disease. Alzheimer's and Dementia: Translational Research and Clinical Interventions, 2019, 5, 492-500.	3.7	5
403	Hippocampal [18F]flortaucipir BPND corrected for possible spill-in of the choroid plexus retains strong clinico-pathological relationships. NeuroImage: Clinical, 2020, 25, 102113.	2.7	5
404	Amyloid burden quantification depends on PET and MR image processing methodology. PLoS ONE, 2021, 16, e0248122.	2.5	5
405	Optimization of injected 68Ga-PSMA activity based on list-mode phantom data and clinical validation. EJNMMI Physics, 2020, 7, 20.	2.7	5
406	Quality control in PET/CT and PET/MRI: Results of a survey amongst European countries. Physica Medica, 2022, 99, 16-21.	0.7	5
407	Application of various iterative reconstruction methods for quantitative 3D dynamic brain PET studies. , 0, , .		4
408	O-145 Prognostic significance of the 18FDG-PET standardized uptake value for inoperable non-small cell lung cancer patients after high-dose radiotherapy. Lung Cancer, 2005, 49, S50.	2.0	4
409	Influence of Outside Field of View Activity on the Quality of High Resolution Research Tomograph (HRRT) Brain studies. , 2006, , .		4
410	Pharmaceutical preparation of oxygen-15 labelled molecular oxygen and carbon monoxide gasses in a hospital setting. Journal of Clinical Pharmacy and Therapeutics, 2010, 35, 63-69.	1.5	4
411	Quantification of the neurokinin 1 receptor ligand [11C]R116301. Nuclear Medicine Communications, 2011, 32, 896-902.	1.1	4
412	Intervention versus standard medical treatment in patients with symptomatic occlusion of the internal carotid artery: a randomised oxygen-15 PET study. EJNMMI Research, 2013, 3, 79.	2.5	4
413	18 F-FDG PET standard uptake values of the normal pons in children: establishing a reference value for diffuse intrinsic pontine glioma. EJNMMI Research, 2014, 4, 8.	2.5	4
414	Design of the NLâ€ENIGMA study: Exploring the effect of Souvenaid on cerebral glucose metabolism in early Alzheimer's disease. Alzheimer's and Dementia: Translational Research and Clinical Interventions, 2016, 2, 233-240.	3.7	4

#	Article	IF	CITATIONS
415	Parametric Method Performance for Dynamic 3′-Deoxy-3′-18F-Fluorothymidine PET/CT in Epidermal Growth Factor Receptor–Mutated Non–Small Cell Lung Carcinoma Patients Before and During Therapy. Journal of Nuclear Medicine, 2017, 58, 920-925.	5.0	4
416	Baseline and longitudinal variability of normal tissue uptake values of [ 18 F]-fluorothymidine-PET images. Nuclear Medicine and Biology, 2017, 51, 18-24.	0.6	4
417	Validation of [18F]FLT as a perfusion-independent imaging biomarker of tumour response in EGFR-mutated NSCLC patients undergoing treatment with an EGFR tyrosine kinase inhibitor. EJNMMI Research, 2018, 8, 22.	2.5	4
418	Quantitative Assessment of Arthritis Activity in Rheumatoid Arthritis Patients Using [11C]DPA-713 Positron Emission Tomography. International Journal of Molecular Sciences, 2020, 21, 3137.	4.1	4
419	Clinically feasible semi-automatic workflows for measuring metabolically active tumour volume in metastatic melanoma. European Journal of Nuclear Medicine and Molecular Imaging, 2021, 48, 1498-1510.	6.4	4
420	Feasibility of pharmacokinetic parametric PET images in scaled subprofile modelling using principal component analysis. NeuroImage: Clinical, 2021, 30, 102625.	2.7	4
421	Aberrant patterns of PET response during treatment for DLBCL patients with MYC gene rearrangements. European Journal of Nuclear Medicine and Molecular Imaging, 2021, , 1.	6.4	4
422	The Optimal Timing of Interim 18F-FDG PET in Diffuse Large B-Cell Lymphoma: An Individual Patient Data Meta-Analysis By the Petra Consortium. Blood, 2019, 134, 487-487.	1.4	4
423	Early 18F-FDG PET/CT Evaluation Shows Heterogeneous Metabolic Responses to Anti-EGFR Therapy in Patients with Metastatic Colorectal Cancer. PLoS ONE, 2016, 11, e0155178.	2.5	4
424	Alzheimer's disease pattern derived from relative cerebral flow as an alternative for the metabolic pattern using SSM/PCA. EJNMMI Research, 2022, 12, .	2.5	4
425	Synthesis and pet-studies of (R)-and (S)-[11C]verapamil for measuring PGP function in MDR1A(+/+)/B(+/+) and MDR1A(-/-)/B(-/-) mice. Journal of Labelled Compounds and Radiopharmaceuticals, 2001, 44, S313-S315.	1.0	3
426	Quantification of dynamic brain studies with the high resolution research tomograph. , 0, , .		3
427	Image properties of various ML-based reconstructions of very noisy HRRT data. , 2011, , .		3
428	Reply to: Area under the cumulative SUV-volume histogram is not a viable metric of intratumoral metabolic heterogeneity. European Journal of Nuclear Medicine and Molecular Imaging, 2013, 40, 1469-1470.	6.4	3
429	The need for quantitative PET in multicentre studies. Clinical and Translational Imaging, 2014, 2, 277-280.	2.1	3
430	18FDG SUV in the primary tumor and lymph node metastases is not predictive for development of distant metastases in high risk head and neck cancer patients. Oral Oncology, 2015, 51, 536-540.	1.5	3
431	Impact of New Scatter Correction Strategies on High-Resolution Research Tomograph Brain PET Studies. Molecular Imaging and Biology, 2016, 18, 627-635.	2.6	3
432	Pancreatic Uptake by 18F-FDOPA PET/CT in Patients With Hypoglycemia After Gastric Bypass Surgery Compared With Controls With or Without Carbidopa Pretreatment. Clinical Nuclear Medicine, 2017, 42, 163-168.	1.3	3

#	Article	IF	CITATIONS
433	Baseline PET as prognostic marker for Hodgkin?. Blood, 2018, 131, 3-4.	1.4	3
434	Volume of interest delineation techniques for 18F-FDG PET-CT scans during neoadjuvant extremity soft tissue sarcoma treatment in adults: a feasibility study. EJNMMI Research, 2018, 8, 42.	2.5	3
435	Performance Evaluation of a Semi-automated Method for [18F]FDG Uptake in Abdominal Visceral Adipose Tissue. Molecular Imaging and Biology, 2019, 21, 159-167.	2.6	3
436	Binding characterization of N â€(2â€chloroâ€5â€thiomethylphenyl)―N ′â€(3â€[ 3 H] 3 methoxy phenyl)―N ′â€methylguanidine ([ 3 H] GMOM ), a nonâ€competitive N â€methylâ€Dâ€aspartate ( NMDA ) receptor antag Pharmacology Research and Perspectives, 2019, 7, e00458.		3
437	P1.04-12 Tumor Uptake and Biodistribution of 89Zr-Labeled Pembrolizumab in Patients with Metastatic Non-Small-Cell Lung Cancer. Journal of Thoracic Oncology, 2019, 14, S443.	1.1	3
438	Interlesional Heterogeneity of Metastatic Neuroendocrine Tumors Based on 18F-DOPA PET/CT. Clinical Nuclear Medicine, 2019, 44, 612-619.	1.3	3
439	Pharmacokinetic Modeling of ( <i>R</i> )-[ <sup>11</sup> C]verapamil to Measure the P-Glycoprotein Function in Nonhuman Primates. Molecular Pharmaceutics, 2021, 18, 416-428.	4.6	3
440	Validation and test–retest repeatability performance of parametric methods for [11C]UCB-J PET. EJNMMI Research, 2022, 12, 3.	2.5	3
441	Noise sensitivity of 89Zr-Immuno-PET radiomics based on count-reduced clinical images. EJNMMI Physics, 2022, 9, 16.	2.7	3
442	In vivo dosimetry with a liquid-filled electronic portal imaging device. Medical Physics, 1998, 25, 2483-2483.	3.0	2
443	Peroperative Neuromonitoring during Carotid Endarterectomy in Relation to Preoperative Positron Emission Tomography Findings. European Journal of Vascular and Endovascular Surgery, 2008, 35, 652-660.	1.5	2
444	Quantitative Issues in Response Measurement by PET. PET Clinics, 2008, 3, 5-11.	3.0	2
445	Prediction of functional recovery after revascularization in patients with chronic ischemic myocardial dysfunction. Nuclear Medicine Communications, 2011, 32, 1169-1173.	1.1	2
446	EORTC Imaging Group. European Journal of Cancer, Supplement, 2012, 10, 82-87.	2.2	2
447	Effects of Reusing Baseline Volumes of Interest by Applying (Non-)Rigid Image Registration on Positron Emission Tomography Response Assessments. PLoS ONE, 2014, 9, e87167.	2.5	2
448	Metabolically active tumour volume segmentation from dynamic [18F]FLT PET studies in non-small cell lung cancer. EJNMMI Research, 2015, 5, 26.	2.5	2
449	Prediction of disease-free survival using relative change in FDG-uptake early during neoadjuvant chemoradiotherapy for potentially curable esophageal cancer: A prospective cohort study. Ecological Management and Restoration, 2017, 30, 1-7.	0.4	2
450	An automatic delineation method for bone marrow absorbed dose estimation in 89Zr PET/CT studies. EJNMMI Physics, 2016, 3, 13.	2.7	2

#	Article	IF	CITATIONS
451	Parametric Methods for Dynamic 11C-Phenytoin PET Studies. Journal of Nuclear Medicine, 2017, 58, 479-483.	5.0	2
452	Reply: Repeatability of Quantitative Whole-Body 18F-FDG PET/CT Uptake Measures in Patients with Non–Small Cell Lung Cancer: Dynamic Versus Test–Retest Design. Journal of Nuclear Medicine, 2017, 58, 1528.2-1529.	5.0	2
453	Dynamic PET Reconstruction Utilizing a Spatiotemporal 4D De-noising Kernel. , 2018, , .		2
454	Should vascular wall 18F-FDG uptake be adjusted for the extent of atherosclerotic burden?. International Journal of Cardiovascular Imaging, 2020, 36, 545-551.	1.5	2
455	SUVs Are Adequate Measures of Lesional <sup>18</sup> F-DCFPyL Uptake in Patients with Low Prostate Cancer Disease Burden. Journal of Nuclear Medicine, 2021, 62, 1264-1269.	5.0	2
456	Non-invasive Standardised Uptake Value for Verification of the Use of Previously Validated Reference Region for [18F]Flortaucipir and [18F]Florbetapir Brain PET Studies. Molecular Imaging and Biology, 2021, 23, 550-559.	2.6	2
457	Biodistribution of <sup>18</sup> F-FES in patients with metastatic ER+ breast cancer undergoing treatment with Rintodestrant (G1T48), a novel selective estrogen receptor degrader. Journal of Nuclear Medicine, 2021, , jnumed.121.262500.	5.0	2
458	Multi-input spectral analysis for evaluation of the contribution of radioactive metabolites in (R)-[11C]verapamil PET data. Journal of Cerebral Blood Flow and Metabolism, 2005, 25, S629-S629.	4.3	2
459	Effects of reference tissue versus plasma input parametric kinetic modelling on statistical parametric analysis of [11C](R)-PK11195 binding in Alzheimer's disease (AD) and young and old subjects. Journal of Cerebral Blood Flow and Metabolism, 2005, 25, S643-S643.	4.3	2
460	Comparison of various models for analysing [11C]flumazenil studies. Journal of Cerebral Blood Flow and Metabolism, 2005, 25, S660-S660.	4.3	2
461	ImmunoPET imaging with 89Zr-cetuximab in patients with advanced colorectal cancer Journal of Clinical Oncology, 2014, 32, 11102-11102.	1.6	2
462	Whole body PD-L1 PET in patients with NSCLC and melanoma Journal of Clinical Oncology, 2018, 36, 139-139.	1.6	2
463	Reply: Automated Segmentation of TMTV in DLBCL Patients: What About Method Measurement Uncertainty?. Journal of Nuclear Medicine, 2021, 62, 432-432.	5.0	2
464	Bloodâ€circulating EVâ€miRNAs, serum TARC, and quantitative FDGâ€PET features in classical Hodgkin lymphoma. EJHaem, 2022, 3, 908-912.	1.0	2
465	Simulated Annealing in pharmacokinetic modeling of PET neuroreceptor studies: accuracy and precision compared with other optimization algorithms. , 0, , .		1
466	Data-driven volume of interest definition: Benefits and pitfalls. NeuroImage, 2006, 31, T63.	4.2	1
467	Accuracy of 3D acquisition mode for myocardial FDG PET studies using a BGO-based scanner. European Journal of Nuclear Medicine and Molecular Imaging, 2007, 34, 1439-1446.	6.4	1
468	Impact of wavelet based denoising of â€PK11195 time activity curves on accuracy and precision of kinetic analysis. Medical Physics, 2008, 35, 5069-5078.	3.0	1

#	Article	IF	CITATIONS
469	PD-0453: Test-retest repeatability analysis of 18F-FDG PET Radiomics features in NSCLC. Radiotherapy and Oncology, 2013, 106, S176.	0.6	1
470	Magnetic field and PET: Does the effect of magnetic field vary with the intrinsic resolution of PET scanners?. , 2014, , .		1
471	IC-P-109: RATIONALE AND DESIGN OF THE NL-ENIGMA STUDY: A DUTCH 24-WEEK RANDOMISED CONTROLLED STUDY TO EXPLORE THE EFFECT OF NUTRITIONAL INTERVENTION ON BRAIN GLUCOSE METABOLISM IN EARLY ALZHEIMER DISEASE. , 2014, 10, P61-P61.		1
472	Reply: Simplified Methods for Quantification of <sup>18</sup> F-Fluoromethylcholine Uptake: Is SUV <sub>AUC,PP</sub> Actually an SUV?. Journal of Nuclear Medicine, 2015, 56, 1806.2-1807.	5.0	1
473	Improving the signal-to-noise ratio in static PET reconstruction using HYPR-OSEM. , 2016, , .		1
474	ICâ€Pâ€182: EVENTâ€BASED MODELING OF THE TEMPORAL ORDERING OF REGIONAL βâ€AMYLOID DEPOSITION BRAIN. Alzheimer's and Dementia, 2018, 14, P152.	I IN THE	1
475	P2â€445: EVENTâ€BASED MODELING OF THE TEMPORAL ORDERING OF REGIONAL βâ€AMYLOID DEPOSITION IN BRAIN. Alzheimer's and Dementia, 2018, 14, P887.	THE 0.8	1
476	PET/CT and PET/MR Tomographs: Image Acquisition and Processing. , 2019, , 199-217.		1
477	Supporting data for positron emission tomography-based risk modelling using a fixed-instead of a relative thresholding method for total metabolic tumor volume determination. Data in Brief, 2020, 28, 104976.	1.0	1
478	18f-FDG PET/CT Baseline Rdiomics Features Improve the Prediction of Treatment Outcome in Diffuse Large B-Cell Lymphoma Patients. Blood, 2020, 136, 27-28.	1.4	1
479	Improving accuracy and precision of PET pharmacokinetic analysis using wavelet based denoising of time activity curves. Journal of Cerebral Blood Flow and Metabolism, 2005, 25, S640-S640.	4.3	1
480	Feasibility of deriving CBF, OEF and CMRO2 from a single dynamic PET scan using a short inhalation of oxygen-15 labelled molecular oxygen. Journal of Cerebral Blood Flow and Metabolism, 2005, 25, S671-S671.	4.3	1
481	Standardization of Imaging Biomarkers: The FDG PET/CT Example. , 2017, , 227-240.		1
482	Baseline Metabolic Tumor Volume in 18FDG-PET-CT Scans in Classical Hodgkin Lymphoma Using Semi-Automatic Segmentation. Blood, 2019, 134, 4049-4049.	1.4	1
483	3D Convolutional Neural Network-Based Denoising of Low-Count Whole-Body 18F-Fluorodeoxyglucose and 89Zr-Rituximab PET Scans. Diagnostics, 2022, 12, 596.	2.6	1
484	In how many kinetic classes can [ <sup>11</sup> C]-(R)-PK11195 brain PET data be segmented?. , 2008, , .		0
485	Implementation of physiological gating on the high resolution research tomograph. , 2008, , .		0
486	O4â€03â€01: Differential impact of apolipoprotein E genotype on distributions of amyloid load and glucose metabolism in Alzheimer's disease. Alzheimer's and Dementia, 2012, 8, P618.	0.8	0

#	Article	IF	CITATIONS
487	EFOMP and EANM: joint recommendations for a curriculum for the education and training of physicists in nuclear medicine. European Journal of Nuclear Medicine and Molecular Imaging, 2013, 40, 645-648.	6.4	0
488	P.4.032 Neuroinflammation in temporal cortex in schizophrenia patients. European Neuropsychopharmacology, 2013, 23, S93-S94.	0.7	0
489	P1-385: RATIONALE AND DESIGN OF THE NL-ENIGMA STUDY, A DUTCH 24-WEEK RANDOMISED CONTROLLED STUDY TO EXPLORE THE EFFECT OF A NUTRITIONAL INTERVENTION ON BRAIN GLUCOSE METABOLISM IN EARLY ALZHEIMER'S DISEASE. , 2014, 10, P455-P456.		0
490	Evaluation of the accuracy of the average Mu-values within patients from MR derived Mu-maps. , 2015, ,		0
491	Effects of boundary conditions in TOF-MLAA reconstruction for PET/MR. , 2015, , .		0
492	Evaluation of a more optimal initial attenuation image estimate in TOF-MLAA for PET/MR. , 2015, , .		0
493	ICâ€Pâ€196: Quantification of TAU Load Using [ <sup>18</sup> F]AVâ€1451 and PET. Alzheimer's and Dementia, 2016, 12, P141.	0.8	0
494	P4â€215: Quantification of Tau Load Using [ <sup>18</sup> F]AVâ€1451 and Pet. Alzheimer's and Dementia, 2016, 12, P1109.	0.8	0
495	158P: PET/CT based imaging biomarkers for response prediction of stage IV NSCLC treated with paclitaxel–carboplatin–bevacizumab with or without nitroglycerin. Journal of Thoracic Oncology, 2016, 11, S126-S127.	1.1	0
496	[P2–387]: EPISODIC MEMORY IN MILD COGNITIVE IMPAIRMENT INVERSELY CORRELATES WITH THE PATIENT CONTRIBUTION TO CEREBRAL BLOOD FLOW NETWORK MODULARITY. Alzheimer's and Dementia, 2017, 13, P777.	0.8	0
497	[P4–235]: PARAMETRIC IMAGING OF TAU LOAD IN ALZHEIMER's PATIENTS AND CONTROLS USING FLORTAUCIPIR. Alzheimer's and Dementia, 2017, 13, P1364.	0.8	0
498	[ICâ€Pâ€206]: PARAMETRIC IMAGING OF TAU LOAD IN ALZHEIMER's PATIENTS AND CONTROLS USING FLORTAUCIPIR. Alzheimer's and Dementia, 2017, 13, P150.	0.8	0
499	A MR Guided De-noising for PET Using IHYPR-LR. , 2017, , .		0
500	Performance Improvements in HYPR-OSEM. , 2017, , .		0
501	Reply: Should we assess repeatability of PET quantitative uptake measurements of each 18F-labelled tracer?. European Journal of Nuclear Medicine and Molecular Imaging, 2018, 45, 1274-1275.	6.4	0
502	ICâ€₽â€111: [ <sup>18</sup> F]FLORBETAPIRâ€SPECIFIC BINDING IN RELATION TO COGNITION IN SUBJECTIVE COGNITIVE DECLINE. Alzheimer's and Dementia, 2018, 14, P95.	0.8	0
503	ICâ€Pâ€⊋22: [18F]AV1451 PET IN RELATION TO ATROPHY ACROSS THE ALZHEIMER'S DISEASE SPECTRUM. Alzheimer's and Dementia, 2018, 14, P180.	0.8	0
504	P3â€438: PARAMETRIC IMAGING OF [ <sup>18</sup> F]FLORBETAPIR: A TESTâ€RETEST STUDY IN HEALTHY SUBJE AND PATIENTS WITH ALZHEIMER'S DISEASE. Alzheimer's and Dementia, 2018, 14, P1281.	cJ.§	0

**RONALD BOELLAARD** 

#	Article	IF	CITATIONS
505	P2â€360: [ <sup>18</sup> F]AV1451 PET IN RELATION TO ATROPHY ACROSS THE ALZHEIMER'S DISEASE SPECTRUM. Alzheimer's and Dementia, 2018, 14, P827.	0.8	0
506	O2â€06â€01: [ <sup>18</sup> F]FLORBETAPIR SPECIFIC BINDING IN RELATION TO COGNITION IN SUBJECTIVE COGNITIVE DECLINE. Alzheimer's and Dementia, 2018, 14, P630.	0.8	0
507	O2â€09â€05: EXTENSION AND VALIDATION OF AN AMYLOID STAGING MODEL: ASSOCIATIONS WITH CLINICAL MEASURES. Alzheimer's and Dementia, 2018, 14, P643.	0.8	0
508	[1122] Quantitative molecular imaging: Can we trust the SUV?. Physica Medica, 2018, 52, 46.	0.7	0
509	Earlyâ€onset Alzheimer's disease is related to differential spatial patterns of tau pathology and cognitive impairment. Alzheimer's and Dementia, 2020, 16, e042041.	0.8	0
510	Quantitative accuracy remains after shortening of dynamic [ 18 F]flortaucipir PET protocol. Alzheimer's and Dementia, 2020, 16, e045710.	0.8	0
511	Regional tau pathology is associated with loss of synapses and reduced synaptic activity: A combined [ 18 F]flortaucipir, [ 11 C]UCBâ€J and magnetoencephalography study. Alzheimer's and Dementia, 2020, 16, e045806.	0.8	0
512	Regional distribution of tau pathology in cognitively unimpaired, genetically identical twins. Alzheimer's and Dementia, 2020, 16, e045876.	0.8	0
513	Generating parametric binding potential and volume of distribution images using a novel 2D basis function method and the two tissue compartment plasma input model. Journal of Cerebral Blood Flow and Metabolism, 2005, 25, S631-S631.	4.3	0
514	Accuracy and quality of parametric CBF, OEF and CMRO2 images: Effects of fixing parameters. Journal of Cerebral Blood Flow and Metabolism, 2005, 25, S610-S610.	4.3	0
515	Does 18F-Fluorodeoxyglucose Outperform 18F-Fluorothymidine When Using Positron Emission Tomography in Predicting Transformation of Indolent Non-Hodgkin's Lymphoma,. Blood, 2011, 118, 3658-3658.	1.4	0
516	MIMEB: A phase II trial to evaluate FDG-PET/FLT-PET and DCE-MRI for early prediction of efficacy in patients with advanced non-small cell lung cancer treated with erlotinib and bevacizumab Journal of Clinical Oncology, 2012, 30, 7603-7603.	1.6	0
517	Utility of PET in Pharmaceutical Development. , 2012, , 1-16.		0
518	MIMEB: A phase II trial to evaluate FDG-PET/FLT-PET, DCE-MRI and molecular biomarkers for early prediction of nonprogression in patients with advanced non-small cell lung cancer treated with erlotinib and bevacizumab Journal of Clinical Oncology, 2014, 32, e19049-e19049.	1.6	0
519	Psychiatric Disorders. , 2016, , 127-138.		0
520	Quality Visits: The EANM/EARL FDG-PET/CT Accreditation Programme. , 2017, , 415-427.		0
521	Evaluation of HYPR-OSEM Using Experimental Phantom and Clinical Patient Data. , 2017, , .		0
522	Inter-site variability of quality control procedures and NEMA image quality in PET/MRI systems. , 2019, 58, .		0

**RONALD BOELLAARD** 

#	Article	IF	CITATIONS
523	Developments in oncological positron emission tomography/computed tomography assessment. Journal of Thoracic Disease, 2015, 7, E637-9.	1.4	0
524	Longitudinal [ <sup>18</sup> F]flortaucipir PET: Comparison of quantitative and semiâ€quantitative parameters. Alzheimer's and Dementia, 2021, 17, .	0.8	0
525	Glioma perfusion quantification with ASL and DSC: head-to-head comparison with 150-H20 PET. Nuklearmedizin - NuclearMedicine, 2022, 61, .	0.7	0
526	Metabolic Tumor Volume for Outcome Prediction in Patients with Aggressive B-Cell Lymphoma Undergoing Chimeric Antigen Receptor T-Cell Therapy. Nuklearmedizin - NuclearMedicine, 2022, 61, .	0.7	0